Available online at www.sciencedirect.com
SCIENCE DIRECT®
Computers and Structures 83 (2005) 69–90
Computers & Structures
www.elsevier.com/locate/compstruc

Insight into finite element shell discretizations by use of the "basic shell mathematical model"

Phill-Seung Lee, Klaus-Jürgen Bathe *

Department of Mechanical Engineering, Massachusetts Institute of Technology, 77 Massachusetts Avenue, Cambridge, MA 02139, United States

Received 12 March 2004; accepted 23 July 2004
Available online 6 November 2004

Abstract

The objective of this paper is to gain insight into finite element discretizations of shells using the basic shell mathematical model and, in particular, regarding the sources of "locking". We briefly review the "basic shell mathematical model" and present a formulation of shell finite elements based on this model. These shell finite elements are equivalent to the widely-used continuum mechanics based shell finite elements. We consider a free hyperboloid shell problem, which is known to be difficult to solve accurately. Using a fine mesh of MITC9 elements based on the basic shell mathematical model, a detailed analysis is performed giving the distributions of all strain terms. A similar analysis using the MITC6 shell element shows why this element locks when the shell thickness is very small.

Keywords: Shell structures; Basic shell mathematical model; MITC shell elements

1. Introduction

Since shell structures are very efficient in carrying loads, they have been frequently used in engineering practice [1,2]. Analytical and numerical analyses of shell structures have been carried out for a very long time. However, in spite of the long history of research on shells, the analysis of shell structures still presents challenges due to difficulties resulting from the complicated and varying behavior (membrane dominated, bending dominated and mixed behaviors) of shells, particularly, when the thickness of a shell is small [2–8].

In practice, the finite element method is the main tool for the analysis of shell structures. Continuum mechanics based shell finite elements have been commonly used for the analysis of general shell structures [1,2]. These discretizations can, in particular, be used generally for both thick and thin shells. However, while the standard displacement based type of shell element usually works well for membrane dominated shell problems, the element is too stiff for bending dominated and mixed problems when the shell is thin. This major difficulty encountered in the finite element analysis of shells is called "locking". Effective finite element discretizations for the analysis of shells should not lock in bending dominated and mixed problems and perform well in

* Corresponding author. Tel.: +1 617 253 6645; fax: +1 617 253 2275.
E-mail address: kjb@mit.edu (K.J. Bathe).

0045-7949/$ - see front matter © 2004 Elsevier Ltd. All rights reserved.
doi:10.1016/j.compstruc.2004.07.005

membrane dominated problems irrespective of the shell thickness.

The use of mixed finite element methods has greatly advanced the field and specifically, mixed interpolated shell finite elements using the MITC (Mixed Interpolation of Tensorial Components) approach proposed in Refs. [9,10] are employed. The technique is effective not only for quadrilateral plate/shell elements but also for triangular plate/shell elements [9–12]. Well-established numerical tests have been performed for the MITC shell finite elements [12–16].

A deeper study of shell structures requires a strong mathematical as well as physical understanding. Shell mathematical models have provided a strong analytical basis for the finite element analysis of shells. Most classical mathematical shell/plate models can be derived from "the basic shell mathematical model" which also is the underlying mathematical model of the continuum mechanics based shell finite elements [2,3]. However, while in the continuum mechanics based shell finite element the three dimensional continuum strain tensor is used, the basic shell mathematical model explicitly provides the membrane, bending and shear strain terms in the form of a shell theory. The study in this paper is motivated by the fact that, to understand the behavior of the continuum mechanics based shell finite elements, we can use the basic shell mathematical model.

Natural steps are then to develop shell finite elements based on the basic shell mathematical model and to analyze the strain terms of that model. This study should enable us to gain insight into finite element discretizations of shells (in particular, when the widely-used continuum mechanics based shell finite elements are employed), and thus help to further identify the sources of locking in finite element solutions.

In the following sections of this paper, we briefly review the basic shell mathematical model and discuss how we interpolate the geometry and the displacements to construct shell finite elements based on this mathematical model. Some numerical tests then show that these shell finite elements are equivalent to the continuum mechanics based shell finite elements. Using a fine mesh of MITC9 elements based on the basic shell mathematical model, the detailed analysis results of a free hyperboloid shell problem are then presented. These results show how the strain terms of the basic shell mathematical model vary in the bending dominated shell structure as the shell thickness decreases. A similar analysis using the MITC6 element gives insight into the locking phenomenon.

2. The basic shell mathematical model

The basic shell mathematical model considered here contains bending, membrane and shear effects. This shell model has the same strain terms that the continuum mechanics based shell finite element formulation implicitly contains. In this section, we provide the geometric concepts and notation used, briefly describe the shell kinematics and present the basic shell mathematical model within the framework of linear elasticity considering an isotropic material. We use the same notation as in Ref. [2].

2.1. Shell geometry

Shells are 3D structures with one dimension, the thickness, small compared to the other two dimensions. This geometric feature is used to define the geometry of shell structures by specifying only the 2D midsurface and the shell thickness. In what follows, the geometric concepts and notation used in the basic shell mathematical model are described.

In order to introduce the definitions of differential geometry, we use the Einstein summation convention. The variables α, β, λ and μ range from 1 to 2 and the variables i, j and k range from 1 to 3.

We consider a shell with a midsurface defined by a 2D chart $\vec{\phi}$, which is an injective mapping from ω into S, see Fig. 1. The covariant base vectors of the midsurface are

$$\vec{a}_\alpha = \frac{\partial \vec{\phi}(\xi^1, \xi^2)}{\partial \xi^\alpha}. \tag{1}$$

The corresponding contravariant base vectors are given by

$$\vec{a}_\alpha \cdot \vec{a}^\beta = \delta^\beta_\alpha, \tag{2}$$

where δ^β_α denotes the Kronecker symbol ($\delta^\beta_\alpha = 1$ if $\beta = \alpha$ and 0 otherwise). We define the unit normal vector to the plane as

$$\vec{a}_3 = \frac{\vec{a}_1 \times \vec{a}_2}{\|\vec{a}_1 \times \vec{a}_2\|}. \tag{3}$$

The 3D geometry of the shell can then be described by the 3D chart given by

$$\vec{\Phi}(\xi^1, \xi^2, \xi^3) = \vec{\phi}(\xi^1, \xi^2) + \xi^3 \vec{a}_3(\xi^1, \xi^2) \tag{4}$$

in the 3D reference domain defined by

$$\Omega = \left\{ (\xi^1, \xi^2, \xi^3) \in \mathbb{R}^3 | (\xi^1, \xi^2) \in \omega, \xi^3 \in \right] -\frac{t}{2}, \frac{t}{2} \left[\right\}, \tag{5}$$

where t is the thickness (assumed here constant) of the shell.

Surface tensors on the midsurface of the shell can now be defined. We define the first fundamental form (2D metric tensor) of the midsurface

$$a_{\alpha\beta} = \vec{a}_\alpha \cdot \vec{a}_\beta \tag{6}$$

or alternatively in contravariant form

$$a^{\alpha\beta} = \vec{a}^\alpha \cdot \vec{a}^\beta. \tag{7}$$

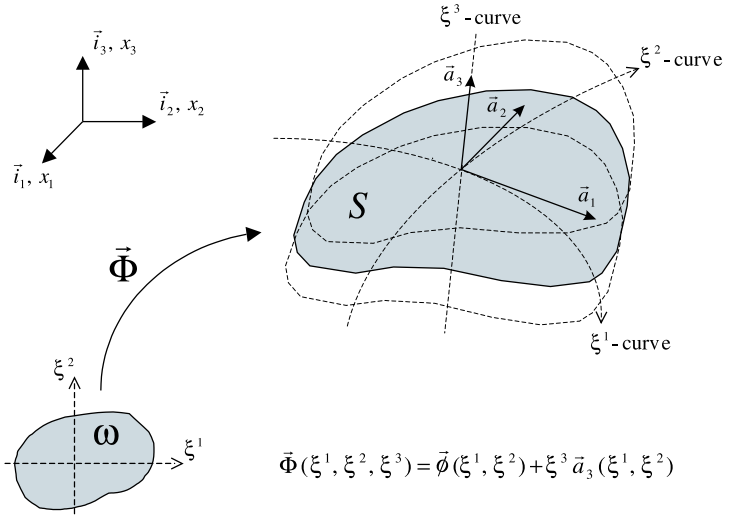

Fig. 1. Geometric description of a shell.

The second fundamental form of the midsurface of the shell is the curvature tensor

$$b_{\alpha\beta} = \vec{a}_3 \cdot \vec{a}_{\alpha,\beta}, \tag{8}$$

which contains all the information on the curvature of the surface. The mixed components of the tensor are

$$b^{\alpha}_{\beta} = a^{\alpha\lambda} b_{\lambda\beta}. \tag{9}$$

We also define the third fundamental form of the surface by

$$c_{\alpha\beta} = b^{\lambda}_{\alpha} b_{\lambda\beta}. \tag{10}$$

The covariant differentiation of a generic surface vector with components w_α on the surface is

$$w_{\alpha|\beta} = w_{\alpha,\beta} - \Gamma^{\lambda}_{\alpha\beta} w_{\lambda}, \tag{11}$$

where $\Gamma^{\lambda}_{\alpha\beta}$ is the surface Christoffel symbol defined by

$$\Gamma^{\lambda}_{\alpha\beta} = \vec{a}_{\alpha,\beta} \cdot \vec{a}^{\lambda}. \tag{12}$$

We can derive the 3D covariant base vectors from Eq. (4),

$$\vec{g}_i = \frac{\partial \vec{\Phi}(\xi^1, \xi^2, \xi^3)}{\partial \xi^i} \tag{13}$$

and then obtain

$$\vec{g}_\alpha = \vec{a}_\alpha - \xi^3 b^{\lambda}_{\alpha} \vec{a}_{\lambda} \tag{14}$$

and

$$\vec{g}_3 = \vec{a}_3. \tag{15}$$

The 3D contravariant base vectors are defined by

$$\vec{g}^i \cdot \vec{g}_j = \delta^i_j. \tag{16}$$

2.2. Shell kinematics

The basic assumption of the shell kinematics is that straight fibers originally normal to the midsurface remain straight and unstretched during the deformation of the shell, which is expressed by

$$\vec{U}(\xi^1, \xi^2, \xi^3) = \vec{u}(\xi^1, \xi^2) + \xi^3 \theta_\lambda(\xi^1, \xi^2) \vec{a}^{\lambda}(\xi^1, \xi^2), \tag{17}$$

where $\vec{u}(\xi^1, \xi^2)$ expresses the infinitesimal translational displacement of the midsurface of the shell and the $\theta_\lambda(\xi^1,\xi^2)$ are the infinitesimal rotations of the material line originally normal to the midsurface, see Fig. 2.

Note that $\theta_\lambda \vec{a}^{\lambda}$ is the rotation vector $\vec{\theta}$ and $\xi^3 \theta_\lambda \vec{a}^{\lambda}$ is the displacement due to the fiber rotation.[1] The translational displacement $\vec{u}$ is also given in the contravariant basis $\vec{a}^1$, $\vec{a}^2$ and $\vec{a}^3 (= \vec{a}_3)$.

For linear analysis, the linear part of the 3D Green–Lagrange strain tensor is used

$$e_{ij} = \frac{1}{2}(\vec{g}_i \cdot \vec{U}_{,j} + \vec{g}_j \cdot \vec{U}_{,i}), \tag{18}$$

where

$$\vec{U}_{,i} = \frac{\partial \vec{U}(\xi^1, \xi^2, \xi^3)}{\partial \xi^i}. \tag{19}$$

Using Eqs. (14) and (15) in Eq. (18), we obtain the covariant components of the strain tensor to be

$$\begin{aligned} e_{\alpha\beta} &= \gamma_{\alpha\beta}(\vec{u}) + \xi^3 \chi_{\alpha\beta}(\vec{u}, \vec{\theta}) - (\xi^3)^2 \kappa_{\alpha\beta}(\vec{\theta}), \\ e_{\alpha 3} &= \zeta_\alpha(\vec{u}, \vec{\theta}), \\ e_{33} &= 0, \end{aligned} \tag{20}$$

[1] Actually, $\vec{\theta}$ is a midsurface vector denoted in Ref. [2] as $\underline{\theta}$.

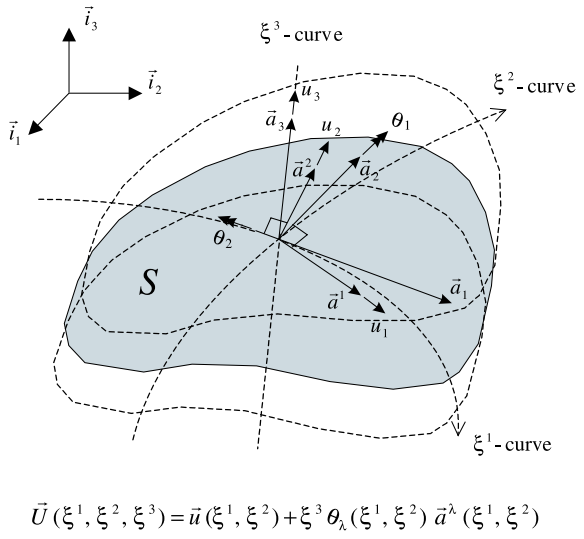

Fig. 2. Shell kinematics.

where

$$\begin{aligned}
\gamma_{\alpha\beta}(\vec{u}) &= \frac{1}{2}(u_{\alpha|\beta}+u_{\beta|\alpha})-b_{\alpha\beta}u_3,\\
\chi_{\alpha\beta}(\vec{u},\vec{\theta}) &= \frac{1}{2}(\theta_{\alpha|\beta}+\theta_{\beta|\alpha}-b^\lambda_\beta u_{\lambda|\alpha}-b^\lambda_\alpha u_{\lambda|\beta})+c_{\alpha\beta}u_3,\\
\kappa_{\alpha\beta}(\vec{\theta}) &= \frac{1}{2}(b^\lambda_\beta\theta_{\lambda|\alpha}+b^\lambda_\alpha\theta_{\lambda|\beta}),\\
\zeta_\alpha(\vec{u},\vec{\theta}) &= \frac{1}{2}(\theta_\alpha+u_{3,\alpha}+b^\lambda_\alpha u_\lambda).
\end{aligned} \tag{21}$$

If we use the plane stress assumption for an isotropic material, that is, the stress normal to the midsurface is zero ($\sigma^{33}=0$), we obtain the constitutive equations

$$\begin{aligned}
\sigma^{\alpha\beta} &= C^{\alpha\beta\lambda\mu}e_{\lambda\mu},\\
\sigma^{\alpha 3} &= \frac{1}{2}D^{\alpha\lambda}e_{\lambda 3}.
\end{aligned} \tag{22}$$

In Eq. (22),

$$C^{\alpha\beta\lambda\mu}=\frac{E}{2(1+\nu)}\left(g^{\alpha\lambda}g^{\beta\mu}+g^{\alpha\mu}g^{\beta\lambda}+\frac{2\nu}{1-\nu}g^{\alpha\beta}g^{\lambda\mu}\right) \tag{23}$$

and

$$D^{\alpha\lambda}=\frac{2E}{1+\nu}g^{\alpha\lambda}, \tag{24}$$

where E and ν are Young's modulus and Poisson's ratio for the material.

Let us now consider a shell structure with zero displacements on a sufficiently large area of the boundary and zero applied traction on the rest of the boundary. Using Eqs. (20)–(24), the governing variational equation for the basic shell mathematical model is:

Find the unknown displacement $\vec{U}$ satisfying the prescribed boundary displacements such that

$$\int_\Omega C^{\alpha\beta\lambda\mu}e_{\alpha\beta}(\vec{U})e_{\lambda\mu}(\vec{V})\mathrm{d}V+\int_\Omega D^{\alpha\lambda}e_{\alpha 3}(\vec{U})e_{\lambda 3}(\vec{V})\mathrm{d}V = \int_\Omega \vec{F}\cdot\vec{V}\mathrm{d}V, \tag{25}$$

where $\vec{V}$ is an arbitrary test function

$$\vec{V}(\xi^1,\xi^2,\xi^3)=\vec{v}(\xi^1,\xi^2)+\xi^3\eta_\lambda(\xi^1,\xi^2)\vec{a}^\lambda(\xi^1,\xi^2), \tag{26}$$

also zero on the boundary of prescribed displacements, and $\vec{F}$ denotes the external loading on the structure.

We only briefly reviewed the basic shell mathematical model, in particular to give explicitly the strain terms in Eqs. (20) and (21) to which we will refer below.

The relation of this model to other shell models is given in Ref. [2]. For further discussions of shell theories relating to continuum mechanics based shell elements, see also Refs. [2,3,17–23] and the references therein.

3. Shell finite elements based on the basic shell mathematical model

Shell finite elements have been frequently formulated using a specific shell theory, see e.g. [17–25]. Of course, this is one of the usual approaches to discretize shell continua using finite element methods. However, as discussed below, when shell finite elements are formulated using a shell theory, care need be exercised in the interpolation of the geometry and displacements to ensure that rigid body motions can be properly represented. This point has of course been mentioned in the literature. However, we shall actually demonstrate below that otherwise significant errors may be observed in the solutions.

In order to construct shell finite elements based on the basic shell mathematical model, we next discuss how to appropriately interpolate the geometry and displacements. Some numerical tests are performed to show the equivalence of the shell finite elements thus developed with the continuum mechanics based shell finite elements. While we seem to consider in this section only displacement-based shell elements, our discussion is of course equally applicable to the development of mixed finite element methods (including the MITC shell elements, see also Section 3.4.2).

3.1. Interpolation of geometry

The interpolation of the shell geometry is easily accomplished using the isoparametric procedure [1]. The 2D chart $\vec{\phi}$ of the discretized domain is given by

$$\vec{\phi}(r,s)=\sum_{i=1}^{q}h_i(r,s)\vec{x}_i, \tag{27}$$

where q is the number of nodes, h_i is the shape function corresponding to node i, and $\vec{x}_i$ is the position vector for

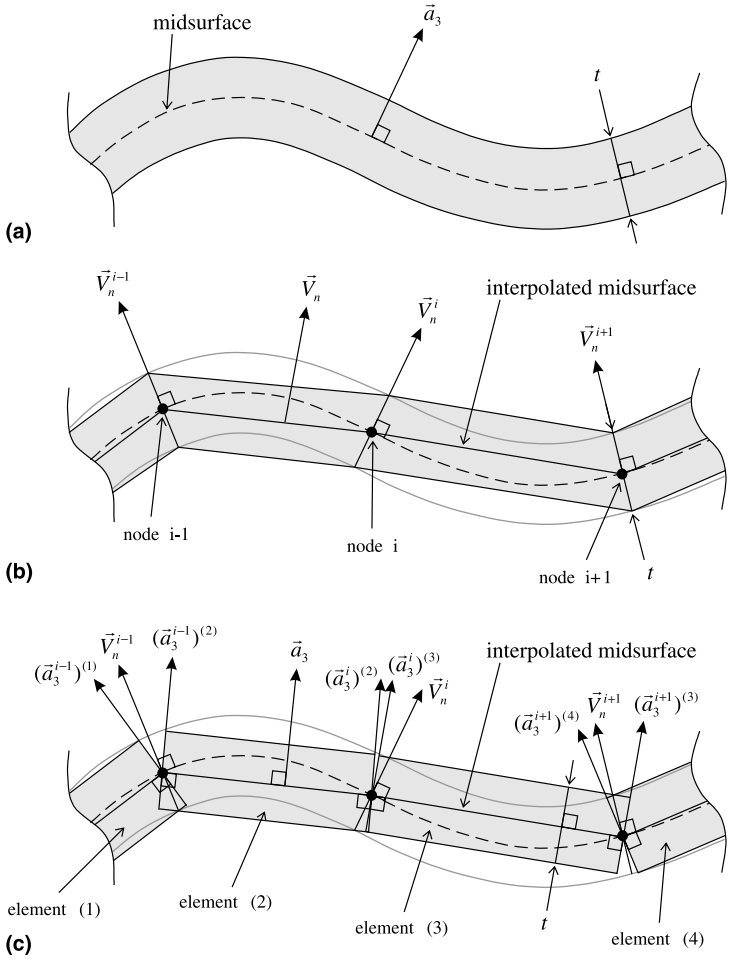

Fig. 3. (a) The physical shell. (b) The discretization using the continuum mechanics based shell finite elements (five degrees of freedom per node). $\vec{V}_n$ is interpolated from the nodal values $\vec{V}_n^i$, which are exactly normal to the midsurface. (c) The discretization using the basic shell mathematical model and Eqs. (46)–(49). $\vec{a}_3$ is calculated to be normal to the interpolated midsurface. The $\vec{V}_n^i$ are the same as in (b) and the same five nodal degrees of freedom are used as for the continuum mechanics based shell finite elements.

node i. The basis of the Cartesian coordinate system, in which $\vec{x}_i$ is defined, is given by the usual unit base vectors $(\vec{i}_1, \vec{i}_2, \vec{i}_3)$. Note that, in this interpolation, we consider the local element coordinates r and s to correspond to ξ^1 and ξ^2 in the basic shell mathematical model we reviewed above. [2]

The covariant base vectors of the interpolated surface are automatically given by

$$\vec{a}_1 = \sum_{i=1}^{q} \frac{\partial h_i}{\partial r}\vec{x}_i, \quad \vec{a}_2 = \sum_{i=1}^{q} \frac{\partial h_i}{\partial s}\vec{x}_i,$$
$$\vec{a}_3 = \frac{\vec{a}_1 \times \vec{a}_2}{\|\vec{a}_1 \times \vec{a}_2\|}. \tag{28}$$

The first fundamental form can be expressed by the matrix [3]

$$[a_{\alpha\beta}] = \begin{bmatrix} \vec{a}_1 \cdot \vec{a}_1 & \vec{a}_1 \cdot \vec{a}_2 \\ \vec{a}_2 \cdot \vec{a}_1 & \vec{a}_2 \cdot \vec{a}_2 \end{bmatrix} \tag{29}$$

or in contravariant form by

$$[a^{\alpha\beta}] = [a_{\alpha\beta}]^{-1}. \tag{30}$$

The contravariant base vectors of the interpolated surface are then calculated by

[2] We assume that there is a one-to-one mapping between (ξ^1, ξ^2) and (r,s), see Ref. [2].

[3] In the following equations, matrices are expressed by brackets and the indices α, β and λ in the brackets do not mean any repetition or summation. As an example, for a tensor equation $c_{\alpha\beta} = a_{\alpha\lambda}b_{\lambda\beta}$, we use the matrix expression $[c_{\alpha\beta}] = [a_{\alpha\beta}][b_{\alpha\beta}]$ instead of $[c_{\alpha\beta}] = [a_{\alpha\lambda}][b_{\lambda\beta}]$.

$$\vec{a}^1 = a^{11}\vec{a}_1 + a^{12}\vec{a}_2,$$
$$\vec{a}^2 = a^{21}\vec{a}_1 + a^{22}\vec{a}_2, \tag{31}$$
$$\vec{a}^3 = \vec{a}_3.$$

We can calculate the second fundamental form of the interpolated surface from Eq. (8),

$$[b_{\alpha\beta}] = \begin{bmatrix} \vec{a}_3 \cdot \sum_{i=1}^{q} \frac{\partial^2 h_i}{\partial r^2}\vec{x}_i & \vec{a}_3 \cdot \sum_{i=1}^{q} \frac{\partial^2 h_i}{\partial r \partial s}\vec{x}_i \\ \vec{a}_3 \cdot \sum_{i=1}^{q} \frac{\partial^2 h_i}{\partial s \partial r}\vec{x}_i & \vec{a}_3 \cdot \sum_{i=1}^{q} \frac{\partial^2 h_i}{\partial s^2}\vec{x}_i \end{bmatrix}. \tag{32}$$

The mixed second fundamental form b^{α}_{β} is obtained from

$$[b^{\alpha}_{\beta}] = [a^{\alpha\beta}][b_{\alpha\beta}]. \tag{33}$$

The third fundamental form of the interpolated surface is

$$[c_{\alpha\beta}] = [b^{\alpha}_{\beta}]^{\mathrm{T}}[b_{\alpha\beta}]. \tag{34}$$

Finally, we obtain the surface Christoffel symbols from

$$[\Gamma^1_{\alpha\beta}] = \begin{bmatrix} \vec{a}^1 \cdot \sum_{i=1}^{q} \frac{\partial^2 h_i}{\partial r^2}\vec{x}_i & \vec{a}^1 \cdot \sum_{i=1}^{q} \frac{\partial^2 h_i}{\partial r \partial s}\vec{x}_i \\ \vec{a}^1 \cdot \sum_{i=1}^{q} \frac{\partial^2 h_i}{\partial s \partial r}\vec{x}_i & \vec{a}^1 \cdot \sum_{i=1}^{q} \frac{\partial^2 h_i}{\partial s^2}\vec{x}_i \end{bmatrix}, \tag{35}$$

$$[\Gamma^2_{\alpha\beta}] = \begin{bmatrix} \vec{a}^2 \cdot \sum_{i=1}^{q} \frac{\partial^2 h_i}{\partial r^2}\vec{x}_i & \vec{a}^2 \cdot \sum_{i=1}^{q} \frac{\partial^2 h_i}{\partial r \partial s}\vec{x}_i \\ \vec{a}^2 \cdot \sum_{i=1}^{q} \frac{\partial^2 h_i}{\partial s \partial r}\vec{x}_i & \vec{a}^2 \cdot \sum_{i=1}^{q} \frac{\partial^2 h_i}{\partial s^2}\vec{x}_i \end{bmatrix}. \tag{36}$$

3.2. Interpolation of displacements

We present here how we obtain the covariant differentiations (see Eq. (11)) of the translational and rotational components in Eq. (21).

As well known, in most shell mathematical models, the midsurface translational displacements are defined in the curvilinear coordinate system,

$$\vec{u} = u_1\vec{a}^1 + u_2\vec{a}^2 + u_3\vec{a}^3. \tag{37}$$

Here the base vectors $\vec{a}^i$ of the displacement vector are functions which depend on the position on the surface. However, in the formulation of isoparametric finite elements, we are using the same interpolation for the geometry and displacements, see e.g. Ref. [1],

$$\vec{u} = \hat{u}_1\vec{i}_1 + \hat{u}_2\vec{i}_2 + \hat{u}_3\vec{i}_3 \tag{38}$$

with

$$\hat{u}_1 = \sum_{i=1}^{q} h_i\hat{u}^i_1, \quad \hat{u}_2 = \sum_{i=1}^{q} h_i\hat{u}^i_2, \quad \hat{u}_3 = \sum_{i=1}^{q} h_i\hat{u}^i_3, \tag{39}$$

where the h_i are the usual shape functions and $\hat{u}^i_1$, $\hat{u}^i_2$ and $\hat{u}^i_3$ are the translational displacement components in the global Cartesian coordinate system at the node i. Using

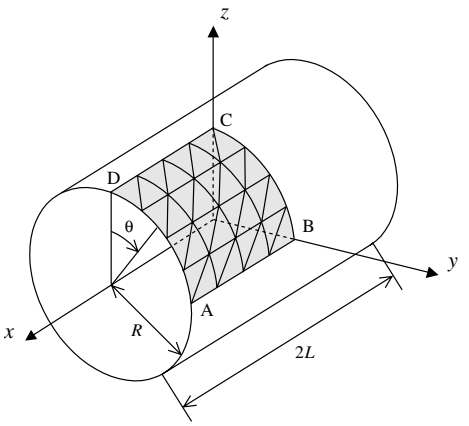

Fig. 4. Cylindrical shell problem with a 4×4 uniform mesh of triangular elements ($L = R = 1.0$, $E = 2.0 \times 10^5$, $\nu = 1/3$ and $p_0 = 1.0$).

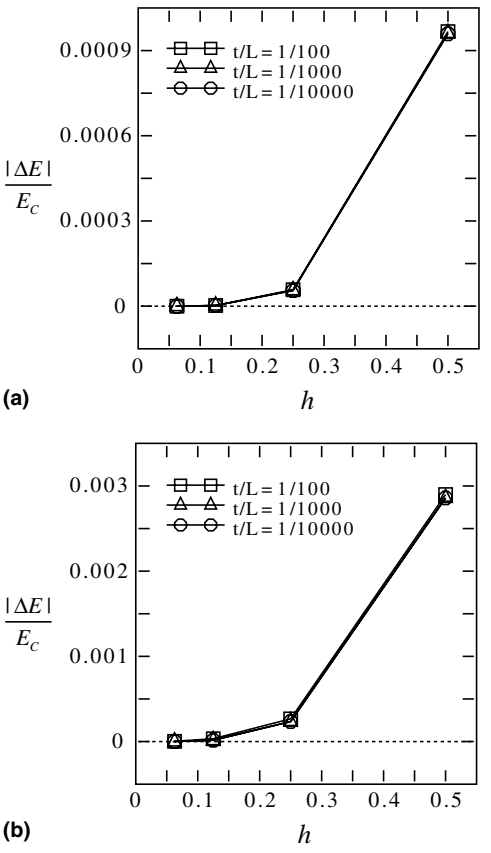

Fig. 5. Strain energy differences between the solutions obtained using the displacement based six-node continuum mechanics based shell finite element and the displacement based six-node shell finite element based on the basic shell mathematical model in the cylindrical shell problems: (a) for clamped case and (b) for free case.

the same interpolation for the geometry and the displacements, the rigid body mode criterion is directly satisfied [1].

Based on Eqs. (37) and (38), we have the transformation relation, implying the Cartesian base vectors,

$$\begin{bmatrix}\hat{u}_1\\ \hat{u}_2\\ \hat{u}_3\end{bmatrix} = [\vec{a}^1 \quad \vec{a}^2 \quad \vec{a}^3]\begin{bmatrix}u_1\\ u_2\\ u_3\end{bmatrix} = \begin{bmatrix}(\vec{a}^1)_1 & (\vec{a}^2)_1 & (\vec{a}^3)_1\\ (\vec{a}^1)_2 & (\vec{a}^2)_2 & (\vec{a}^3)_2\\ (\vec{a}^1)_3 & (\vec{a}^2)_3 & (\vec{a}^3)_3\end{bmatrix}\begin{bmatrix}u_1\\ u_2\\ u_3\end{bmatrix}, \tag{40}$$

where $()_i$ denotes the ith component of the vector in $()$.

We can now calculate the covariant components u_i and their derivatives. Due to the orthonormality between the contravariant and covariant base vectors, we obtain

$$\begin{bmatrix}u_1\\ u_2\\ u_3\end{bmatrix} = \begin{bmatrix}(\vec{a}_1)_1 & (\vec{a}_1)_2 & (\vec{a}_1)_3\\ (\vec{a}_2)_1 & (\vec{a}_2)_2 & (\vec{a}_2)_3\\ (\vec{a}_3)_1 & (\vec{a}_3)_2 & (\vec{a}_3)_3\end{bmatrix}\begin{bmatrix}\hat{u}_1\\ \hat{u}_2\\ \hat{u}_3\end{bmatrix}, \tag{41}$$

where the covariant base vectors are calculated by Eq. (28).

For convenience, we introduce

$$\bar{t}_1 = \begin{bmatrix}(\vec{a}_1)_1\\ (\vec{a}_2)_1\\ (\vec{a}_3)_1\end{bmatrix}, \quad \bar{t}_2 = \begin{bmatrix}(\vec{a}_1)_2\\ (\vec{a}_2)_2\\ (\vec{a}_3)_2\end{bmatrix}, \quad \bar{t}_3 = \begin{bmatrix}(\vec{a}_1)_3\\ (\vec{a}_2)_3\\ (\vec{a}_3)_3\end{bmatrix}. \tag{42}$$

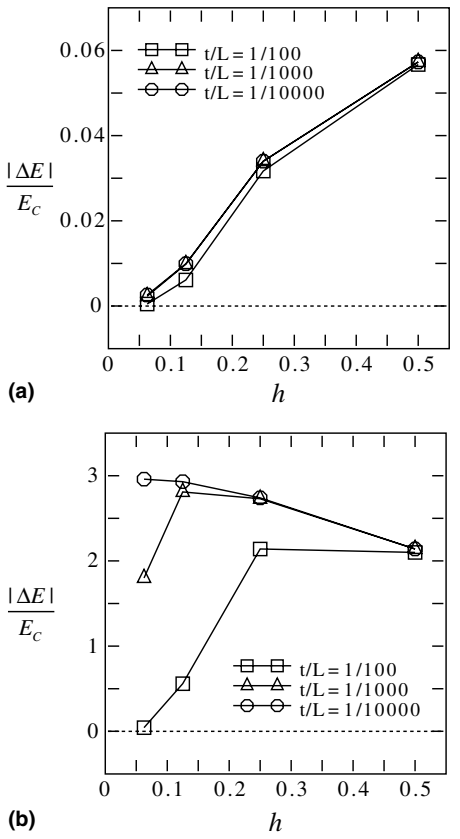

Fig. 6. Strain energy differences between the solutions obtained using the displacement based six-node continuum mechanics based shell finite element and the displacement based six-node shell finite element based on the basic shell mathematical model using the displacement interpolation in Eqs. (51) and (52) in the cylindrical shell problems: (a) for clamped case and (b) for free case.

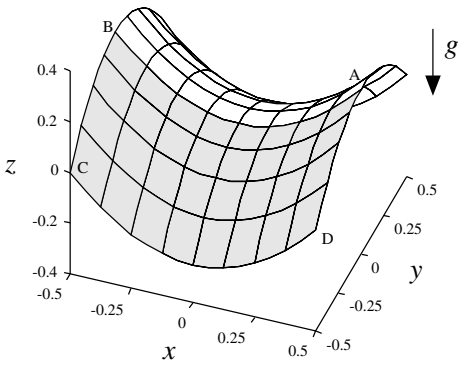

Fig. 7. The 4×8 uniform mesh for half the structure of the partly clamped hyperbolic paraboloid shell problem ($L = 1.0$, $E = 2.0 \times 10^{11}$ and $\nu = 0.3$). The structure is loaded by its self-weight $\rho g t = 80$ per unit surface area.

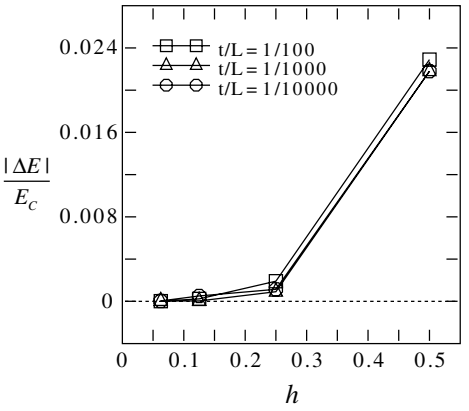

Fig. 8. Strain energy differences between the solutions obtained using the MITC9 continuum mechanics based shell finite element and the MITC9 shell finite element based on the basic shell mathematical model in the partly clamped hyperbolic paraboloid shell problem.

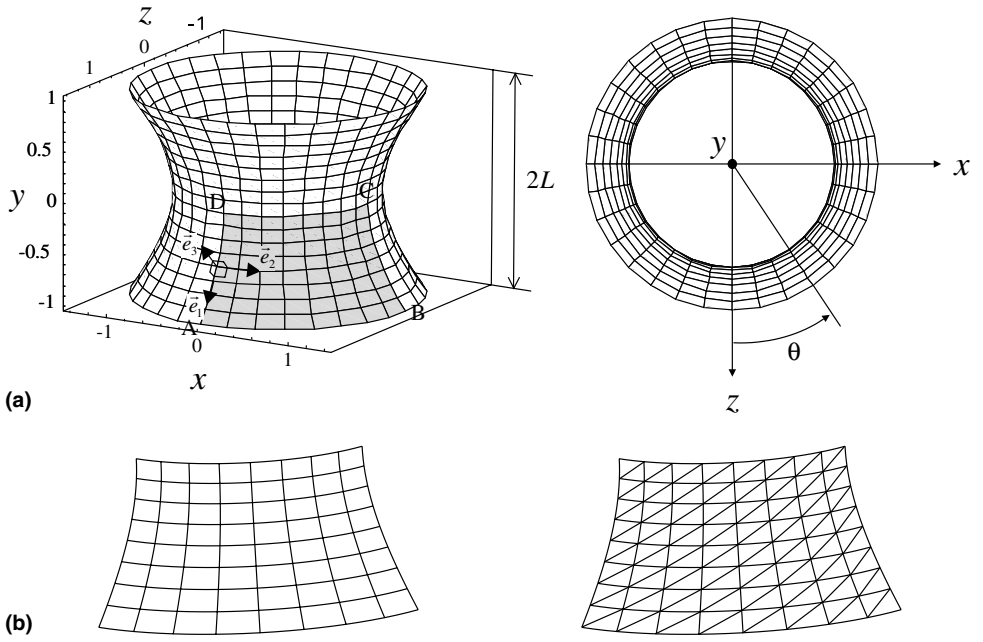

Fig. 9. (a) Hyperboloid shell ($L = 1.0$, $E = 2.0 \times 10^{11}$, $v = 1/3$ and $p_0 = 1.0 \times 10^6$). Computational domain and Cartesian axes used for strain representations. (b) The 8×8 uniform meshes used for the MITC9 and MITC6 shell finite elements.

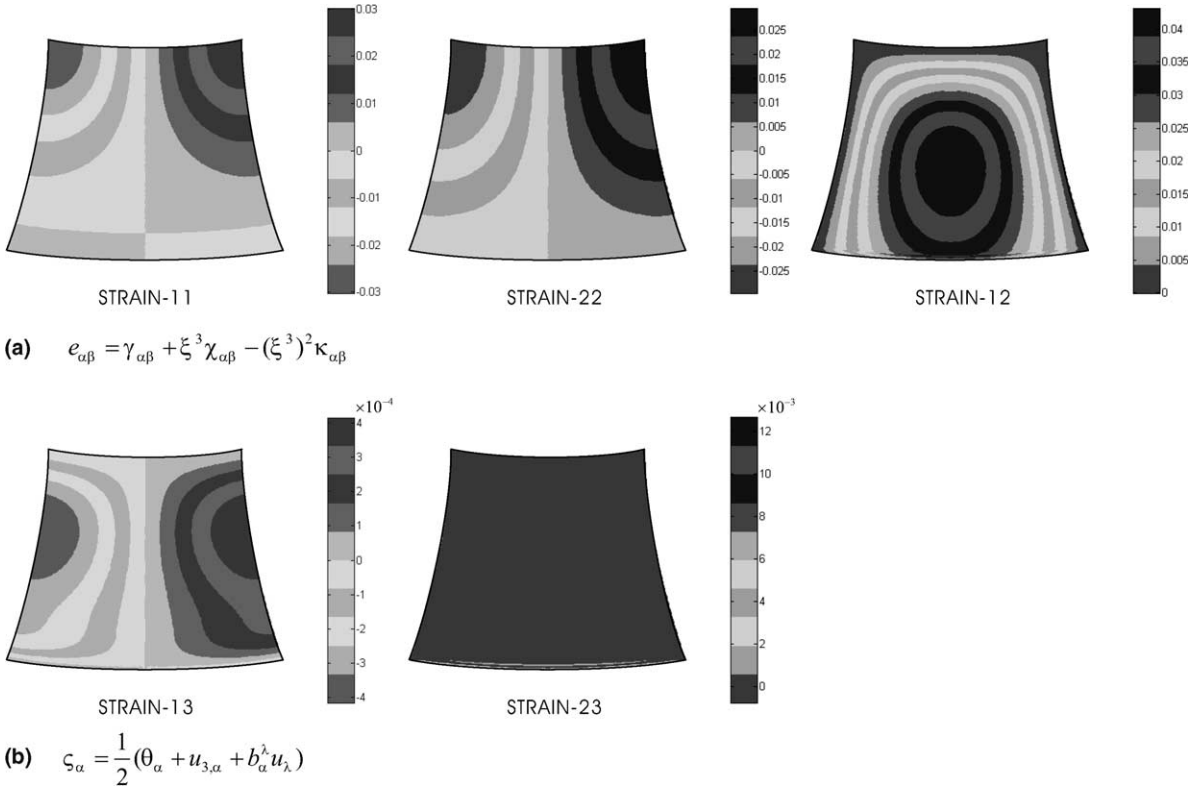

Fig. 10. Reference strain distributions of the free hyperboloid shell problem (MITC9 shell element used, 64×64 mesh, $t/L = 1/100$): (a) reference in-plane strain and (b) reference transverse shear strain.

Then Eq. (41) can be written as

$$\begin{bmatrix} u_1 \\ u_2 \\ u_3 \end{bmatrix} = \hat{u}_i \bar{t}_i \tag{43}$$

and

$$\begin{bmatrix} u_{1,\alpha} \\ u_{2,\alpha} \\ u_{3,\alpha} \end{bmatrix} = (\hat{u}_i)_{,\alpha} \bar{t}_i + \hat{u}_i (\bar{t}_i)_{,\alpha}, \tag{44}$$

in which $\hat{u}_i$ is interpolated by Eq. (39). In order to obtain the transformation relationships for the rotational components and their derivatives, we proceed as for the translational components. Let $\vec{\Theta}$ be the rotation vector defined in the global Cartesian coordinate system,

$$\vec{\Theta} = \Theta_1 \vec{i}_1 + \Theta_2 \vec{i}_2 + \Theta_3 \vec{i}_3. \tag{45}$$

Then as in Eqs. (43) and (44)

$$\begin{bmatrix} \theta_1 \\ \theta_2 \end{bmatrix} = \Theta_i \bar{t}_i^{\theta}, \quad \begin{bmatrix} \theta_{1,\alpha} \\ \theta_{2,\alpha} \end{bmatrix} = (\Theta_i)_{,\alpha} \bar{t}_i^{\theta} + \Theta_i (\bar{t}_i^{\theta})_{,\alpha}, \tag{46}$$

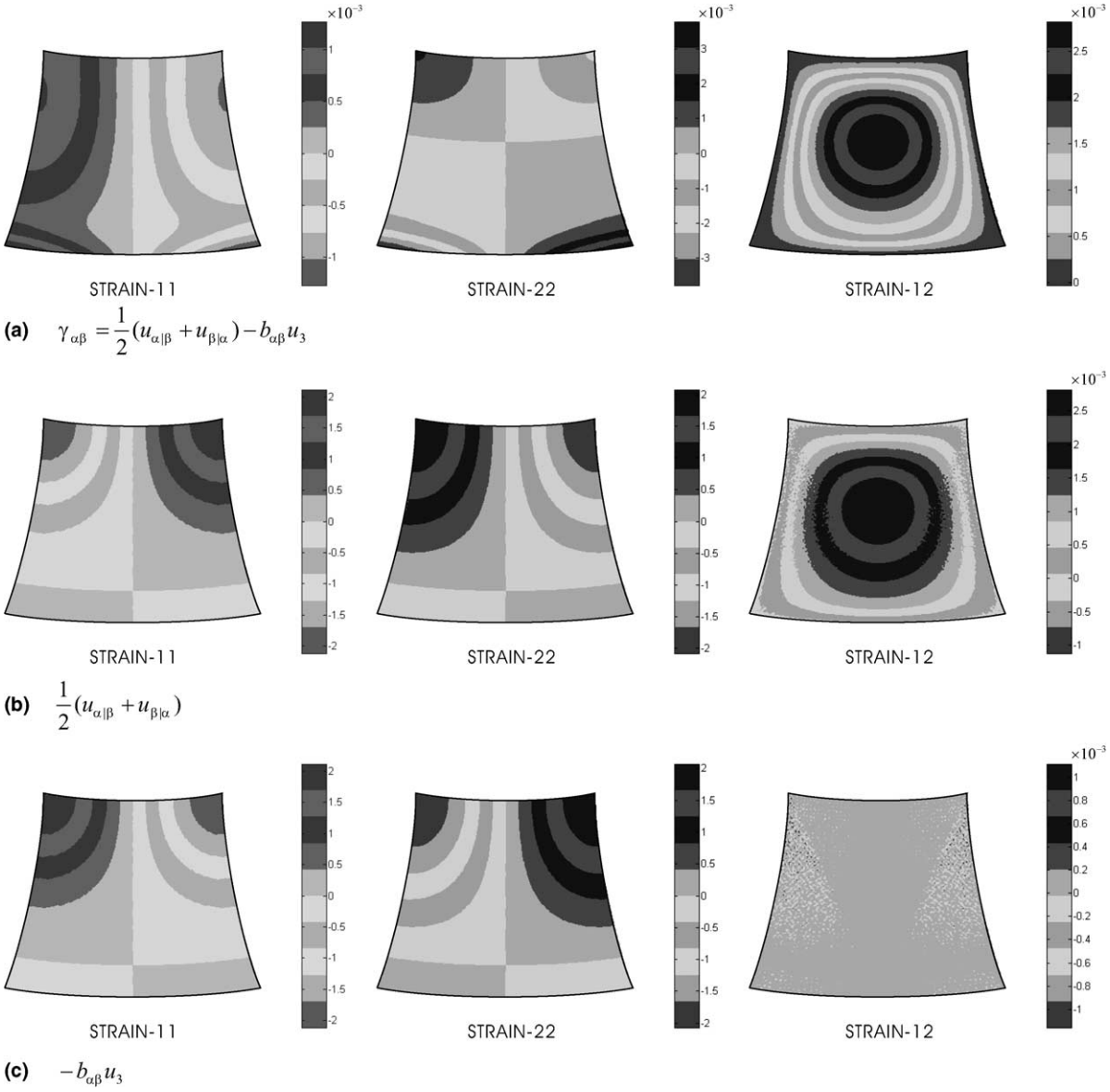

Fig. 11. Reference distributions of the strain components of the free hyperboloid shell problem; $t/L = 1/100$: (a) the membrane strain; (b) the first part of the membrane strain and (c) the second part of the membrane strain.

(a) $\xi^3\chi_{\alpha\beta} = \xi^3\left\{\frac{1}{2}(\theta_{\alpha|\beta} + \theta_{\beta|\alpha} - b^{\lambda}_{\beta}u_{\lambda|\alpha} - b^{\lambda}_{\alpha}u_{\lambda|\beta}) + c_{\alpha\beta}u_3\right\}$

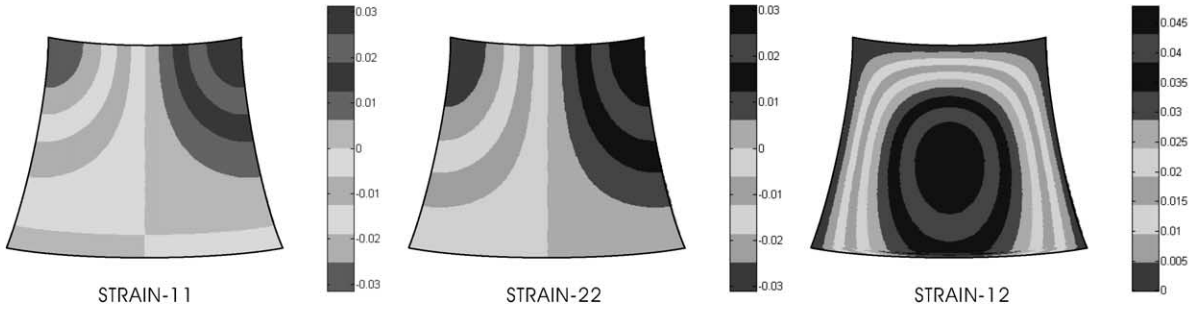

(b) $\frac{1}{2}\xi^3(\theta_{\alpha|\beta} + \theta_{\beta|\alpha})$

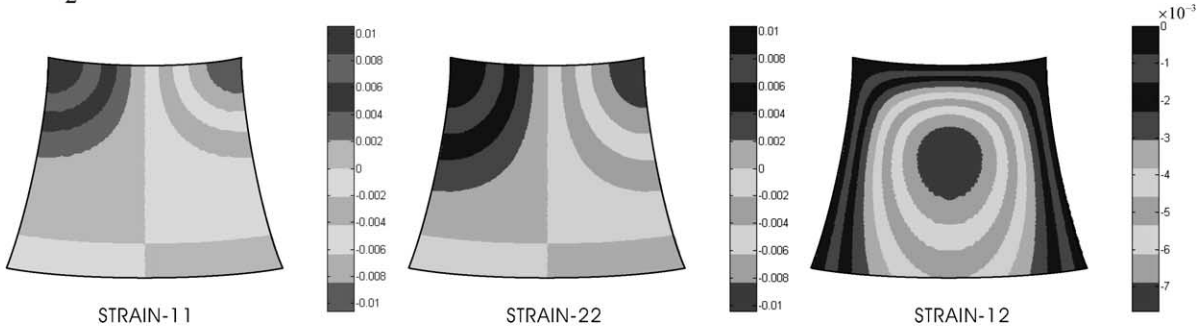

(c) $\frac{1}{2}\xi^3(-b^{\lambda}_{\beta}u_{\lambda|\alpha} - b^{\lambda}_{\alpha}u_{\lambda|\beta})$

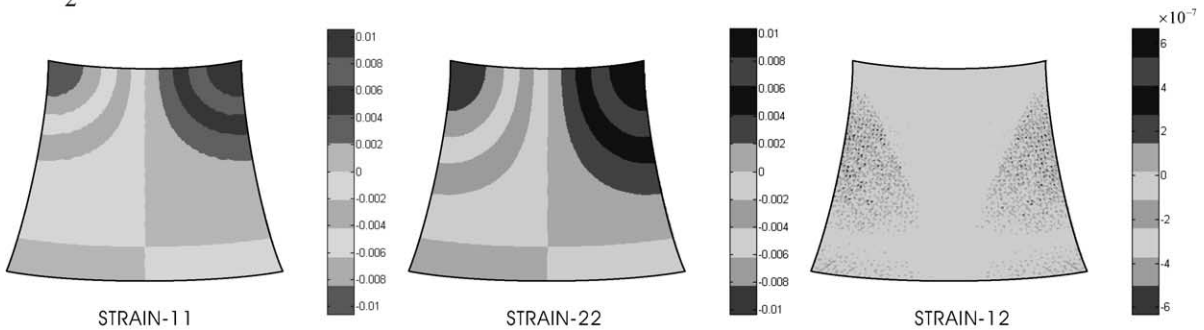

(d) $\xi^3 c_{\alpha\beta}u_3$

Fig. 12. Reference distributions of the strain components of the free hyperboloid shell problem; t/L = 1/100: (a) the first bending strain; (b) the first part of the first bending strain; (c) the second part of the first bending strain and (d) the third part of the first bending strain.

where

$$\bar{t}_1^{\theta} = \begin{bmatrix} (\vec{a}_1)_1 \\ (\vec{a}_2)_1 \end{bmatrix}, \quad \bar{t}_2^{\theta} = \begin{bmatrix} (\vec{a}_1)_2 \\ (\vec{a}_2)_2 \end{bmatrix}, \quad \bar{t}_3^{\theta} = \begin{bmatrix} (\vec{a}_1)_3 \\ (\vec{a}_2)_3 \end{bmatrix} \tag{47}$$

and

$$\Theta_1 = \sum_{i=1}^{q} h_i \Theta_1^i, \quad \Theta_2 = \sum_{i=1}^{q} h_i \Theta_2^i,$$

$$\Theta_3 = \sum_{i=1}^{q} h_i \Theta_3^i. \tag{48}$$

In practice, using the continuum mechanics based shell finite element discretization, we normally employ five degrees of freedom at a node [1,2], and then have

$$\vec{\Theta} = \sum_{i=1}^{q} h_i (-\vec{V}_2^{\,i} \alpha_i + \vec{V}_1^{\,i} \beta_i), \tag{49}$$

where α_i and β_i are the rotations about the vectors $\vec{V}_1^i$ and $\vec{V}_2^i$, respectively. These vectors are derived from the shell nodal director vector $\vec{V}_n^i$, i.e. assuming that $\vec{i}_2$ and $\vec{V}_n^i$ are not parallel,

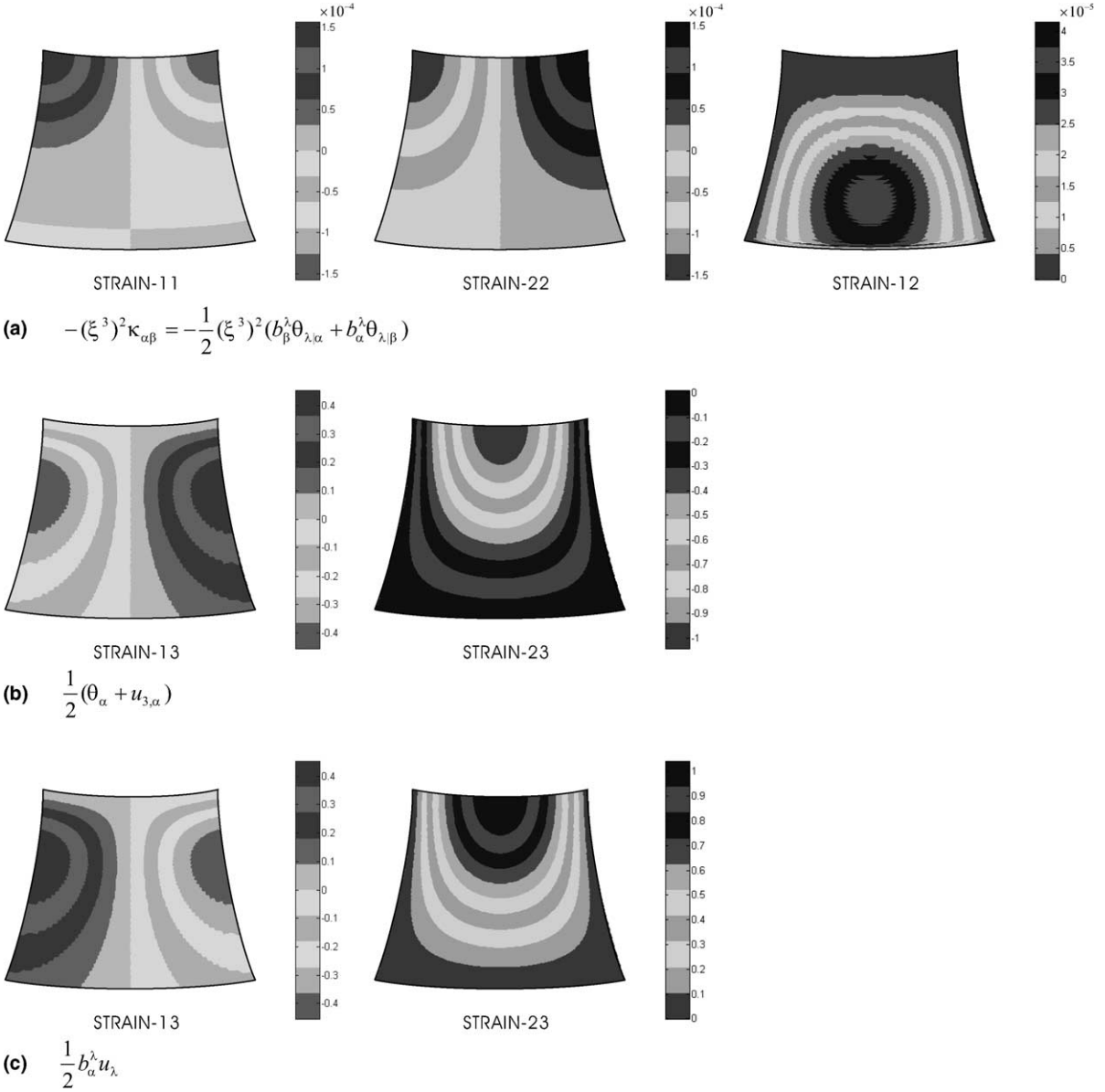

Fig. 13. Reference distributions of the strain components of the free hyperboloid shell problem; $t/L = 1/100$: (a) the second bending strain; (b) the first part of the transverse shear strain and (c) the second part of the transverse shear strain.

$$\vec{V}_1^i = \frac{\vec{i}_2 \times \vec{V}_n^i}{\|\vec{i}_2 \times \vec{V}_n^i\|}, \quad \vec{V}_2^i = \vec{V}_n^i \times \vec{V}_1^i, \tag{50}$$

see Ref. [1], and the director vector is frequently calculated by averaging the midsurface normal vectors $\vec{a}_3$ of the elements sharing node i.

For the continuum mechanics based shell finite element, the director vector in the element $\vec{V}_n$ is interpolated from the nodal director vectors, see Fig. 3, and the element stiffness matrices can then directly be calculated [1]. To develop the shell finite element based on the basic shell mathematical model, we need to decide how to establish $\vec{a}_3$. In our implementation, we calculate $\vec{a}_3$ to be a unit normal vector to the element interpolated midsurface. At the nodes, however, the same nodal director vectors are used as for the continuum mechanics based shell finite elements, but merely to be able to introduce the nodal rotations as given in Eq. (49), see Fig. 3(c). These assumptions of course introduce a difference in the formulations and hence differences in the computed analysis results. But the differences in analysis results can be expected to be small for smooth shell midsurfaces (those we consider, see Sections 3.4 and 4).

The above expressions can now directly be used to evaluate the strain components in Eq. (20).

Note that, alternatively, we could also directly interpolate the covariant components in Eq. (37)

$$u_1 = \sum_{i=1}^{q} h_i u_1^i, \quad u_2 = \sum_{i=1}^{q} h_i u_2^i, \quad u_3 = \sum_{i=1}^{q} h_i u_3^i \tag{51}$$

and similarly

$$\theta_1 = \sum_{i=1}^{q} h_i \theta_1^i, \quad \theta_2 = \sum_{i=1}^{q} h_i \theta_2^i, \tag{52}$$

where the u_1^i, u_2^i and u_3^i are the covariant components of the translational displacement vector at the node i, and the θ_1^i and θ_2^i are the covariant components of the rotation vector at the node i. In this case, it is not necessary to use the transformation mentioned above but care must then be exercised that for any geometric form and size of shell element the rigid body mode criterion is still fulfilled. This point is exemplified in Appendix A. A formulation that does not satisfy the rigid body mode criterion cannot be recommended for general use [1].

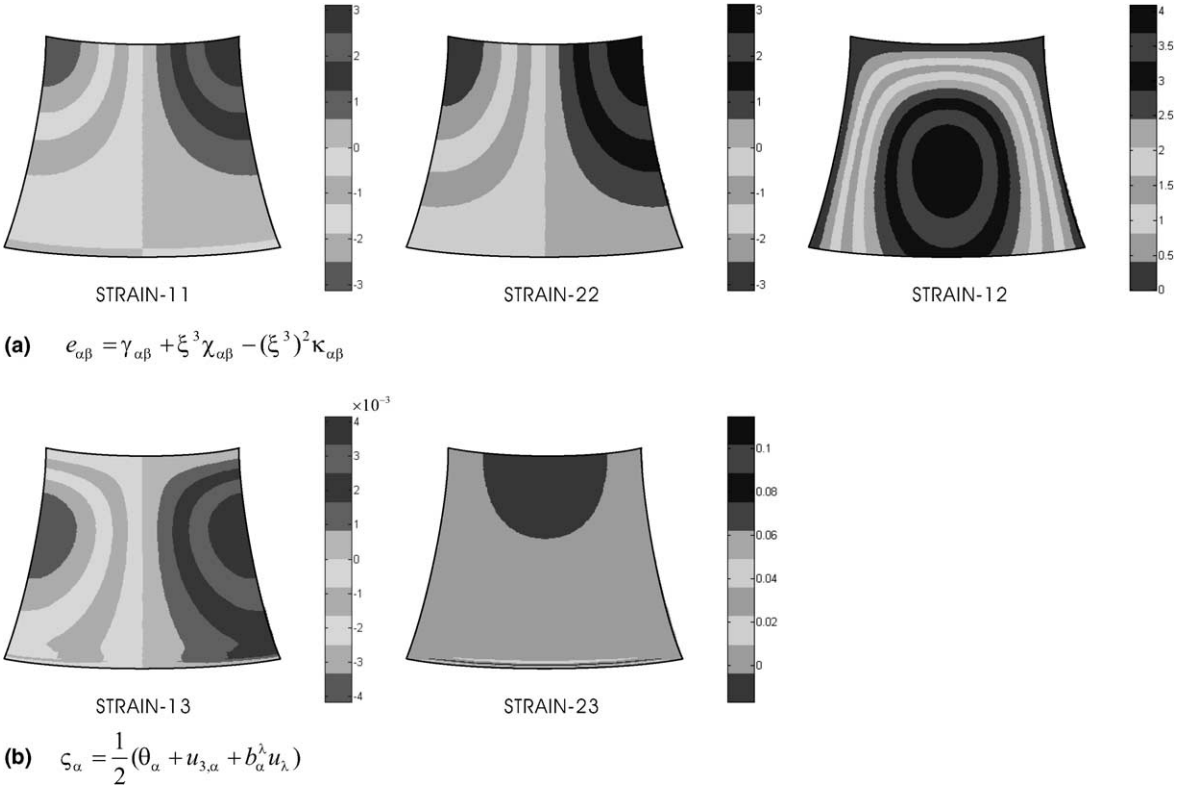

Fig. 14. Reference strain distributions of the free hyperboloid shell problem (MITC9 shell element used, 64×64 mesh, $t/L = 1/1000$): (a) reference in-plane strain and (b) reference transverse shear strain.

3.3. Strain-displacement and stiffness matrices

The final step in the element formulation is to construct the strain-displacement and stiffness matrices. The covariant strain-displacement matrix corresponding to the 3D contravariant basis, defined in Eq. (16), is immediately obtained from Eq. (20) in terms of the nodal displacements and rotations.

For the numerical implementation, it is somewhat involved to use the constitutive relationship in Eq. (22). A more effective way is to obtain the 3D strain components in the global Cartesian coordinate system and employ the usual 3D constitutive relationship with the plane stress assumption imposed as shown, for example, in Ref. [1]. The stiffness matrices of the shell finite elements based on the basic shell mathematical model are then calculated as the stiffness matrices of the continuum mechanics based shell finite elements.

These considerations and conclusions, as those in Section 3.2, are also applicable to the MITC shell elements because of the specific formulation of these elements, see Refs. [1,2,14]. The good convergence

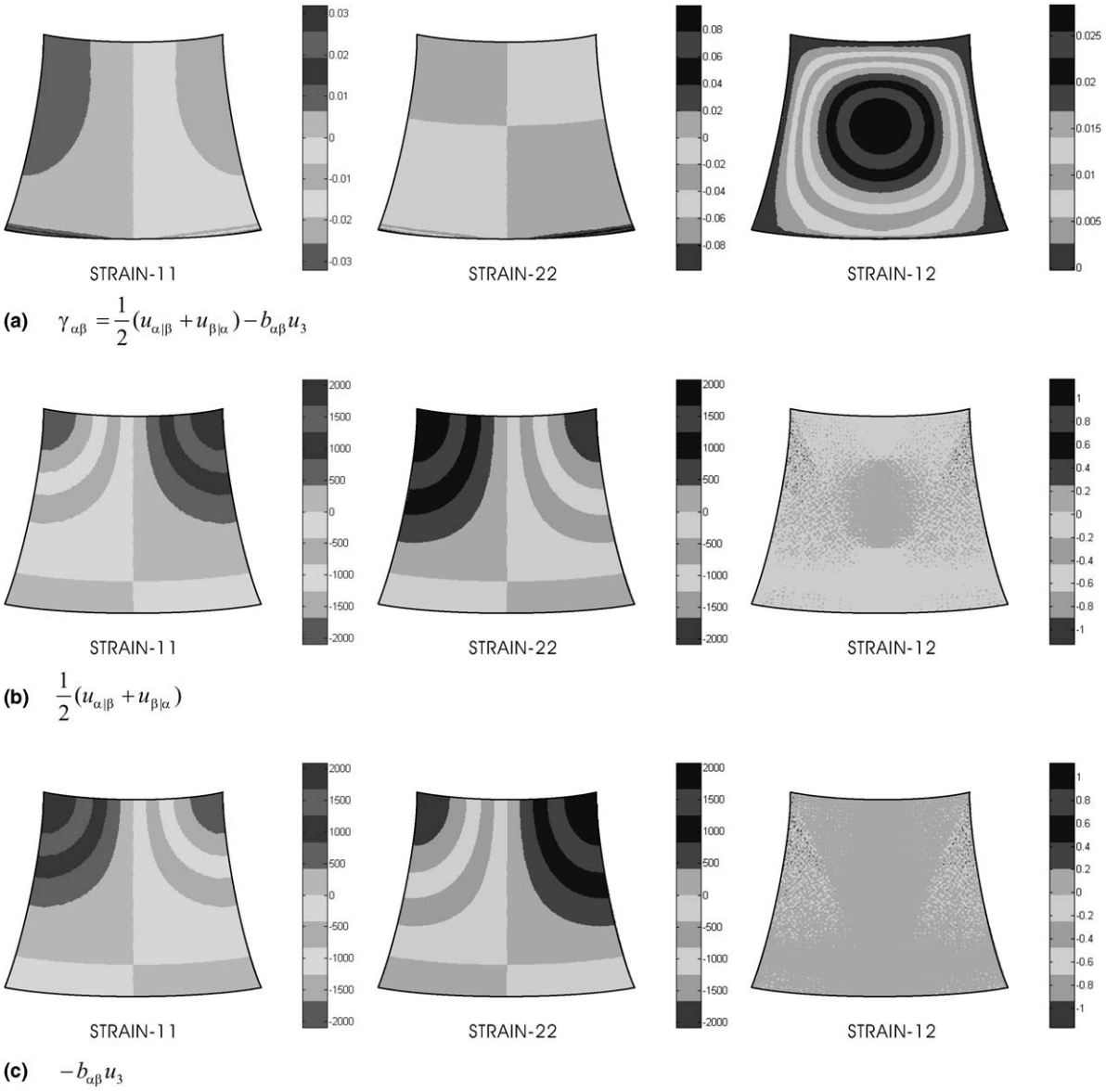

Fig. 15. Reference distributions of the strain components of the free hyperboloid shell problem; t/L = 1/1000: (a) the membrane strain; (b) the first part of the membrane strain and (c) the second part of the membrane strain.

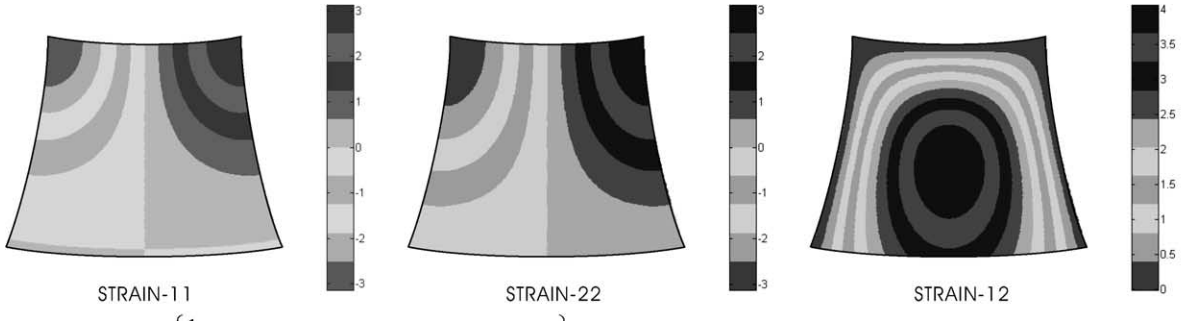

(a) $\xi^3\chi_{\alpha\beta} = \xi^3\left\{\frac{1}{2}(\theta_{\alpha|\beta} + \theta_{\beta|\alpha} - b^{\lambda}_{\beta}u_{\lambda|\alpha} - b^{\lambda}_{\alpha}u_{\lambda|\beta}) + c_{\alpha\beta}u_3\right\}$

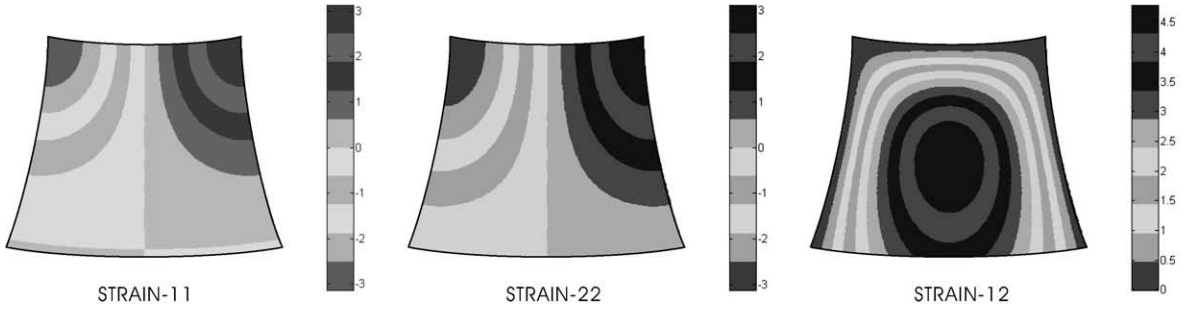

(b) $\frac{1}{2}\xi^3(\theta_{\alpha|\beta} + \theta_{\beta|\alpha})$

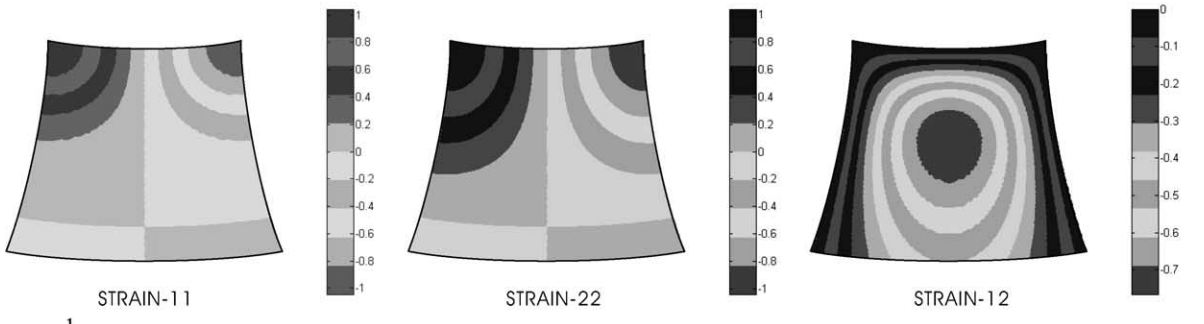

(c) $\frac{1}{2}\xi^3(-b^{\lambda}_{\beta}u_{\lambda|\alpha} - b^{\lambda}_{\alpha}u_{\lambda|\beta})$

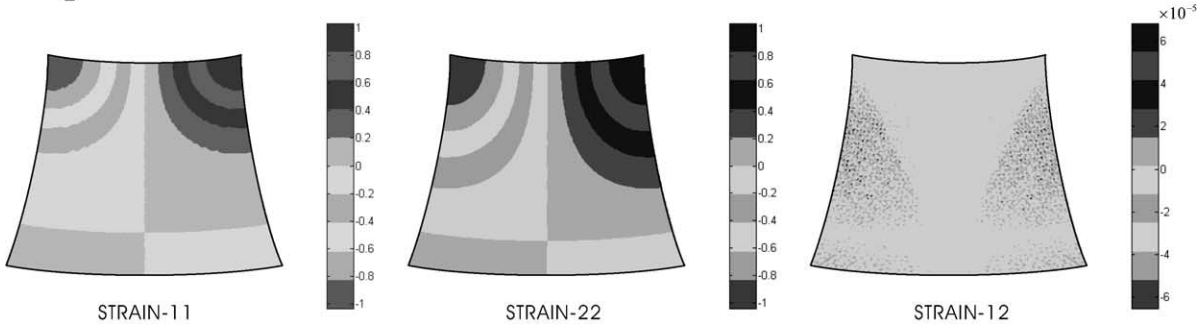

(d) $\xi^3 c_{\alpha\beta}u_3$

Fig. 16. Reference distributions of the strain components of the free hyperboloid shell problem; t/L = 1/1000: (a) the first bending strain; (b) the first part of the first bending strain; (c) the second part of the first bending strain and (d) the third part of the first bending strain.

properties of these elements have been studied, for example, in Refs. [14,16,26].

3.4. Numerical comparisons

To this point, we reviewed the basic shell mathematical model and presented how to formulate a shell finite element discretization based on this model. As we pointed out, small differences must be expected in the solutions compared to those obtained with the continuum mechanics based shell finite elements, because of the assumptions used regarding $\vec{V}_n$ and $\vec{a}_3$ in each of the elements, see Fig. 3. If, however, for the two formulations, the same element nodal points and the same interpolated element midsurfaces are used, and $\vec{a}_3$ is equal to $\vec{V}_n$, for every point in the corresponding elements, then the same element stiffness matrices are obtained. A trivial such case is the analysis of a plate. But also, we must expect that in the analysis of a smooth shell, this condition is always reached as the mesh is refined.

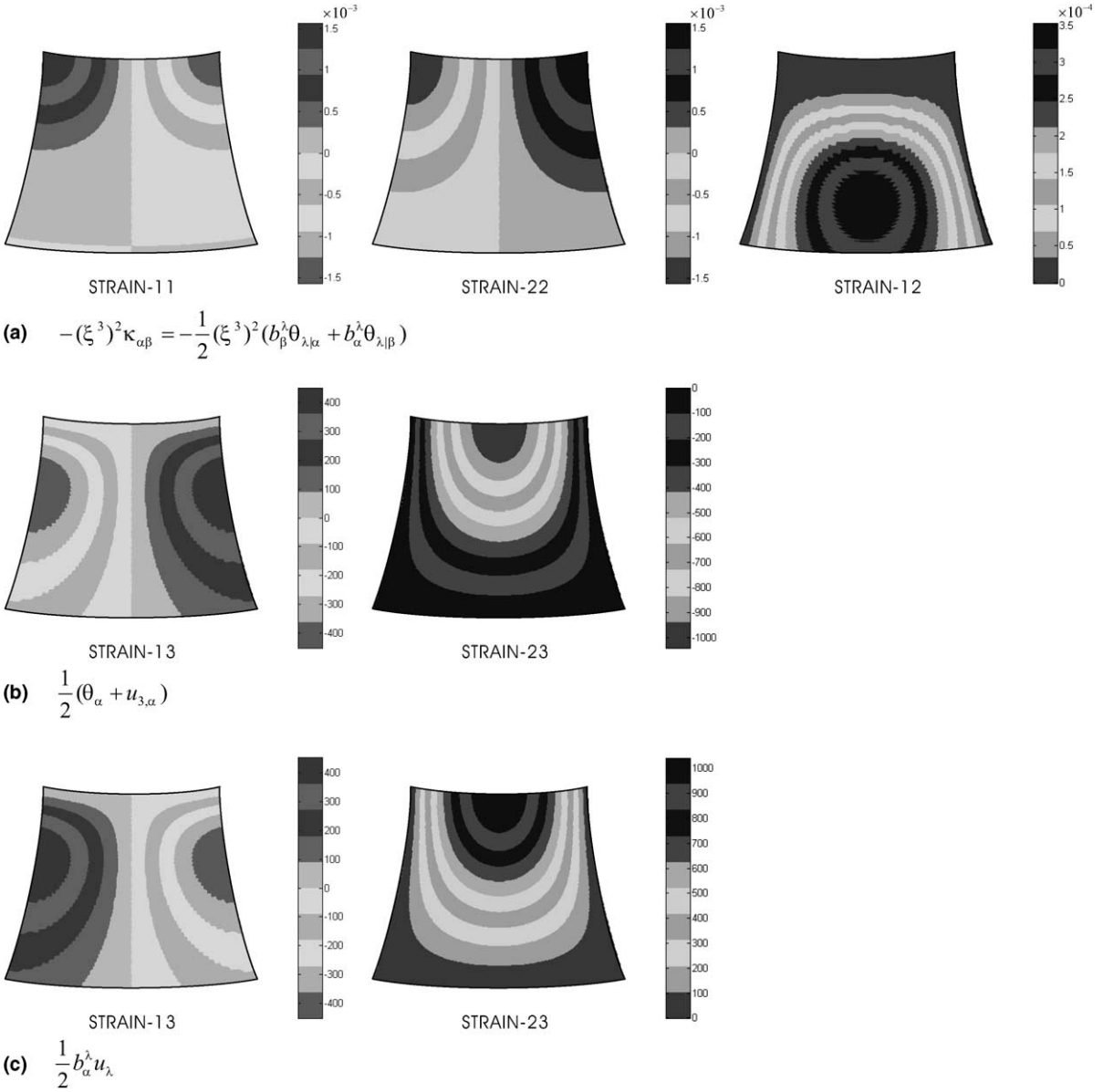

Fig. 17. Reference distributions of the strain components of the free hyperboloid shell problem; $t/L = 1/1000$: (a) the second bending strain; (b) the first part of the transverse shear strain and (c) the second part of the transverse shear strain.

Table 1
Order of the strain magnitudes in the reference solutions calculated using the MITC9 shell finite element based on the basic shell mathematical model. For the membrane strain, the normal strain components ϵ_{11} and ϵ_{22} are considered

t/L	Terms considered on the left-hand side of Eq. (58)		
	$\gamma_{\alpha\beta} = \frac{1}{2}(u_{\alpha\|\beta} + u_{\beta\|\alpha}) - b_{\alpha\beta}u_3$	$\frac{1}{2}(u_{\alpha\|\beta} + u_{\beta\|\alpha})$	$-b_{\alpha\beta}u_3$
1/10	10^{-4}	10^{-3}	10^{-3}
1/100	10^{-3}	10^{+0}	10^{+0}
1/1000	10^{-2}	10^{+3}	10^{+3}
	$\zeta_\alpha = \frac{1}{2}(\theta_\alpha + u_{3,\alpha} + b^\lambda_\alpha u_\lambda)$	$\frac{1}{2}(\theta_\alpha + u_{3,\alpha})$	$\frac{1}{2}(b^\lambda_\alpha u_\lambda)$
1/10	10^{-5}	10^{-4}	10^{-4}
1/100	10^{-4}	10^{-1}	10^{-1}
1/1000	10^{-3}	10^{+2}	10^{+2}

In this section we demonstrate numerically by means of some examples that indeed even when using relatively coarse meshes, this difference is very small and that therefore the formulations are equivalent. Note that in these example solutions we do not measure the accuracy of the response predicted (compared to an exact or highly accurate solution) but only the difference in the response predicted using the two formulations.

We also show in this section that it is important to interpolate the displacements as discussed in Section 3.2 (i.e. the rigid body mode criterion must be satisfied).

3.4.1. Cylindrical shell problems

We consider the well known cylindrical shell problems described in Fig. 4. The shell has uniform thickness t, length $2L$ and radius R and is subjected to the pressure distribution $p(\theta)$ normal to the shell surface

$$p(\theta) = p_0 \cos(2\theta). \tag{53}$$

Depending on whether both ends are clamped or free, the asymptotic behavior of the structure is membrane dominated or bending dominated, respectively. By symmetry, the analyses are performed using one eighth of the structure, the shaded region ABCD in Fig. 4. The detailed description of the shell problems is presented in Refs. [12,14].

Using the continuum mechanics based shell finite element and the shell finite element based on the basic shell mathematical model, we compare the strain energy difference of the solutions obtained using the displacement based 6-node elements for both the membrane dominated and bending dominated shell problems as the element size h decreases. To investigate the dependence of the difference on the shell thickness, we consider the cases $t/L = 1/100$, $t/L = 1/1000$ and $t/L = 1/10000$. The difference is calculated by

$$\frac{|\Delta E|}{E_C} = \frac{|E_C - E_B|}{E_C}, \tag{54}$$

where E_C and E_B denote the strain energies of the solutions obtained with the continuum mechanics based shell finite element and the shell finite element based on the basic shell mathematical model, respectively.

Fig. 5(a) and (b) report that for the clamped and free cases the strain energy differences between the solutions obtained using the two shell finite elements quickly vanish independent of the shell thickness as the element size decreases. Note that, when the element size is as large as $L/2$ ($h = 0.5$, that is, a 2×2 mesh is used.), the energy difference is already less than 0.1% and 0.3% for the clamped and free cases, respectively.

We perform similar numerical tests for the shell finite element based on the basic shell mathematical model using the displacement interpolation in Eqs. (51) and (52). Fig. 6(a) and (b) shows that, when we use the displacement interpolation in Eqs. (51) and (52), as exemplified in the Appendix A, the results using the shell finite element based on the basic shell mathematical model are very different to the results using the continuum mechanics based shell finite element for the free case and small shell thickness. Actually, the calculated strain energy is much too large. This is due to the fact that rigid body motions are not contained in the element formulation (see Appendix A). The need to be able to represent the rigid body modes is strikingly important in the case of the free cylinder and small shell thickness.

3.4.2. Partly clamped hyperbolic paraboloid shell problem

The partly clamped hyperbolic paraboloid shell problem shown in Fig. 7 is a good bending dominated benchmark problem to test a formulation for locking, see Refs. [2,5,14]. The shell surface is defined by

$$z = x^2 - y^2; \quad (x, y) \in \left[-\frac{1}{2}, \frac{1}{2}\right]^2 \tag{55}$$

and clamped along the side $x = -1/2$.

The structure is loaded by its self-weight ($\rho g t = 80$ per unit surface area). By symmetry, we can limit calculations to the shaded region ABCD in Fig. 7 with clamped boundary conditions along BC and symmetry

conditions along AB. The detailed solution results and an asymptotic analysis are given in Refs. [5,14].

Using Eq. (54), we calculate the strain energy difference between the solutions obtained using the MITC9 continuum mechanics based shell finite element and the MITC9 shell finite element based on the basic shell mathematical model (for the MITC9 shell element see Ref. [26]). Fig. 8 displays the rapidly decreasing difference between the two shell finite element solutions as the element size decreases.

4. Detailed study of shell finite element discretizations

As discussed above, the shell finite elements based on the basic shell mathematical model are equivalent to the continuum mechanics based shell finite elements. We next use the shell finite elements based on the basic shell mathematical model to perform a detailed study of the strain components in finite element discretizations as obtained using either discretization approach as the shell thickness decreases.

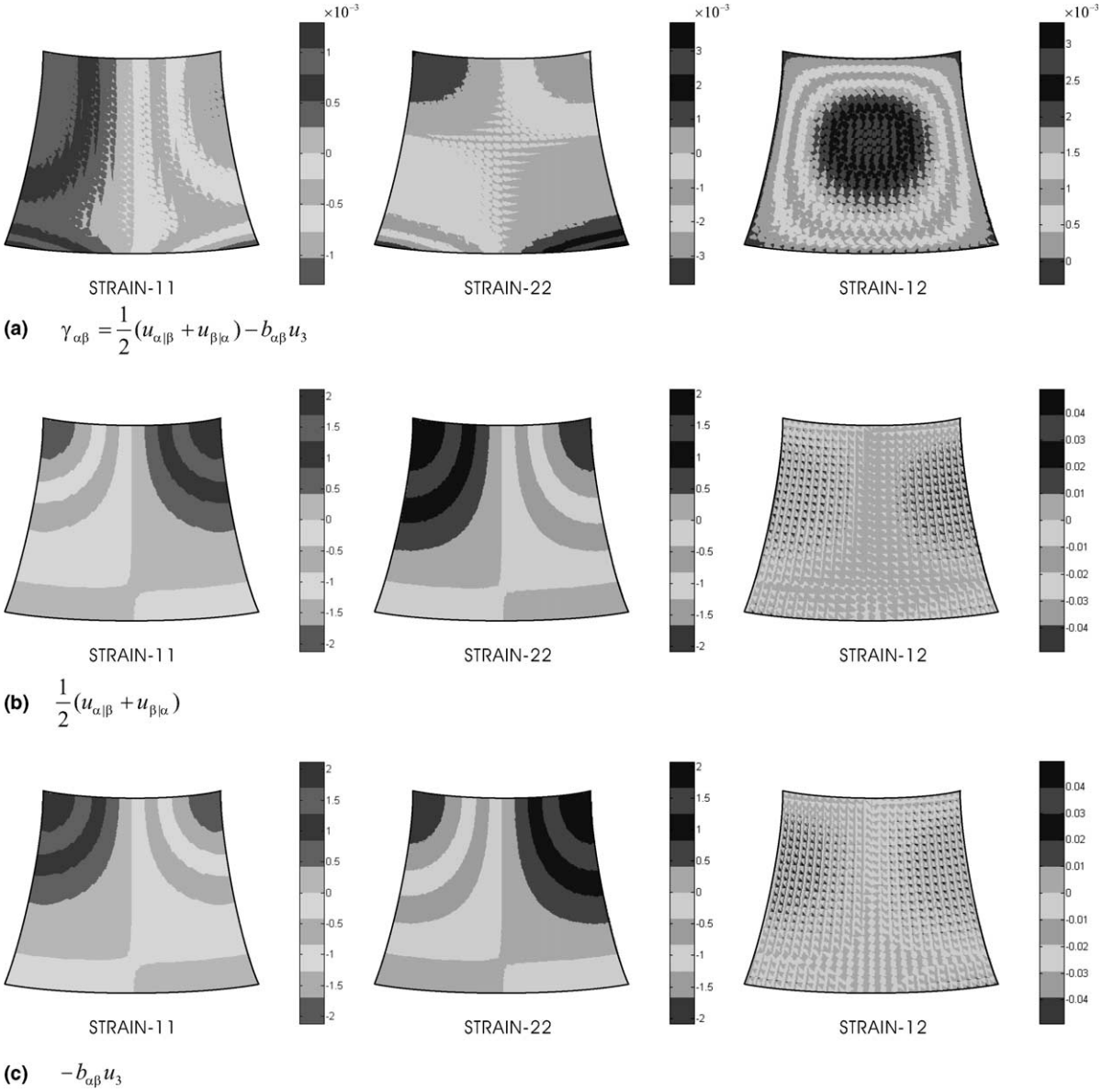

Fig. 18. Distributions of the strain components of the free hyperboloid shell problem calculated using the MITC6 shell element with a 24×24 mesh, $t/L = 1/100$: (a) the membrane strain; (b) the first part of the membrane strain and (c) the second part of the membrane strain.

The hyperboloid shell shown in Fig. 9 is considered. The midsurface of this shell is described by

$$x^2 + z^2 = 1 + y^2; \quad y \in [-1, 1]. \tag{56}$$

The loading imposed is the smoothly varying periodic pressure normal to the surface,

$$p(\theta) = p_0 \cos(2\theta). \tag{57}$$

A bending dominated problem is obtained when both ends are free and a membrane dominated problem is obtained when the ends are clamped. However, we consider here only the bending dominated case, in which membrane and shear locking can occur. By symmetry, the shaded region ABCD shown in Fig. 9 is used for the calculations.

This is a difficult bending dominated problem to solve when the thickness is small, but the problem is a good test case because of the negative Gaussian curvature of the shell surface, see Refs. [12,26]. The objective of this detailed study is to identify some of the difficulties that arise in the finite element solution of this shell problem.

We consider two thickness ratios, namely $t/L = 1/100$ and $t/L = 1/1000$, which are common thickness ratios encountered in engineering practice. All parts of the strain components in Eqs. (20) and (21) of the basic shell mathematical model are considered.

We should note that, although the strain components and their parts in Eqs. (20) and (21) are covariant components in the curvilinear coordinate system, the strain distributions plotted in all figures correspond to the local Cartesian shell-aligned coordinate system [1] and at the outer surface ($\xi^3 = t/2$) of the hyperboloid shell. The plotted strains are also unsmoothed [1]. The relationship between the strains in the different coordinate systems is

$$\begin{aligned} e_{\alpha\beta}(\vec{g}^{\alpha} \otimes \vec{g}^{\beta}) &= \epsilon_{\lambda\mu}(\vec{e}_{\lambda} \otimes \vec{e}_{\mu}), \\ e_{\alpha 3}(\vec{g}^{\alpha} \otimes \vec{g}^{3}) &= \epsilon_{\beta 3}(\vec{e}_{\beta} \otimes \vec{e}_{3}), \end{aligned} \tag{58}$$

where $e_{\alpha\beta}$ and $e_{\alpha 3}$ are the covariant strain components or their parts in the curvilinear coordinate system, and $\epsilon_{\alpha\beta}$ and $\epsilon_{\alpha 3}$ are the strain components plotted in the local Cartesian shell-aligned coordinate system defined by the base vectors $\vec{e}_i$ (see Fig. 9 [1]).

4.1. Detailed strain analysis using the MITC9 shell element

The free hyperboloid shell problem was solved using a uniform 64×64 mesh of the MITC9 shell element (of course, based on the basic shell mathematical model).

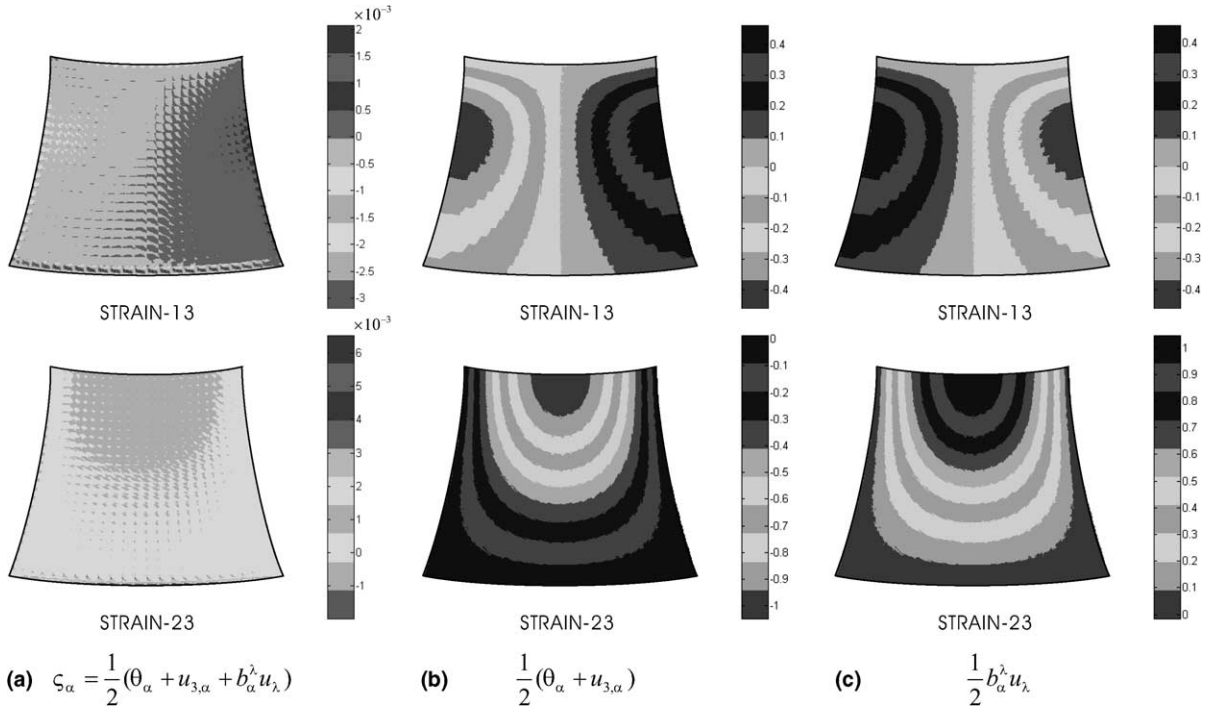

Fig. 19. Distributions of the strain components of the free hyperboloid shell problem calculated using the MITC6 shell element; $t/L = 1/100$: (a) the transverse shear strain; (b) the first part of the transverse shear strain and (c) the second part of the transverse shear strain.

This solution is deemed accurate [26] and provides reference strain distributions.

Figs. 10–13 and 14–17 show the reference strain distributions when t/L is 1/100 and 1/1000. These figures not only show the total strain components but also individual parts.

It is important to see that, as the shell thickness decreases, there is an increasing difference in the orders of magnitudes between the membrane strain and its two parts, see Figs. 11 and 15. These figures show that both parts of the membrane strain are of opposite sign and in absolute values about three and five orders of magnitudes larger than the total membrane strain itself. A similar phenomenon is seen for the transverse shear strains and their individual parts, see Figs. 10(b), 13(b) and (c), 14(b) and 17(b) and (c).

Table 1 summarizes the orders of the strain magnitudes in the reference solutions when the thickness ratios are 1/10, 1/100 and 1/1000. The order of the membrane strain is 10 times smaller than of its parts when $t/L = 1/10$ but 10^5 times smaller when $t/L = 1/1000$. The same ratios also hold for the orders of the transverse shear strains.

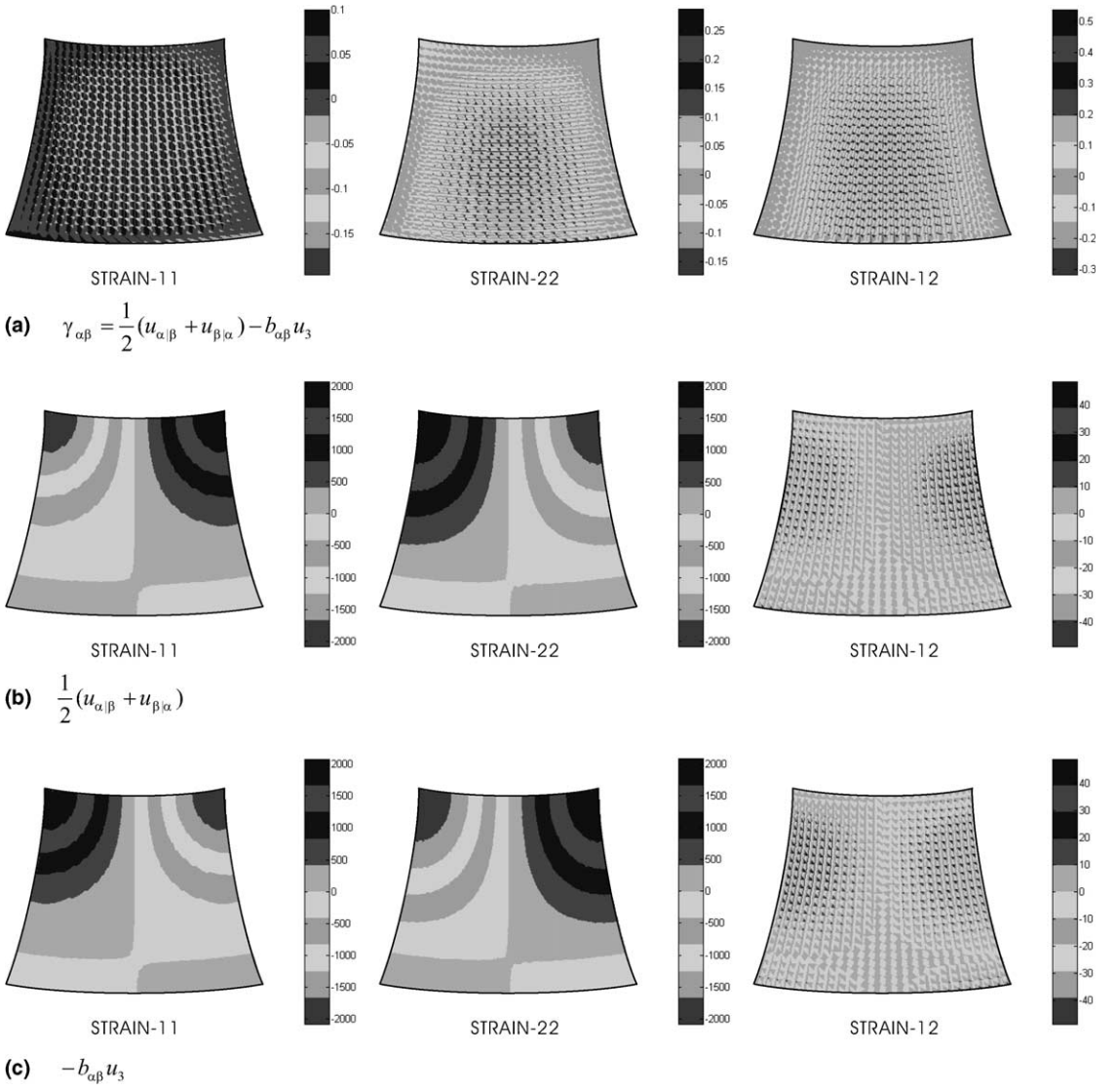

Fig. 20. Distributions of the strain components of the free hyperboloid shell problem calculated using the MITC6 shell element with a 24×24 mesh, $t/L = 1/1000$: (a) the membrane strain; (b) the first part of the membrane strain and (c) the second part of the membrane strain.

In a numerical solution, it is difficult to calculate accurately a small value by summing two very large values and, as the two values grow, the difficulty increases. Clearly, this difficulty can be a major source of errors in the numerical solution of the shell problem. Indeed, as the shell thickness decreases, the increasing difference in the orders of the magnitudes between the membrane strain and its two parts can be a source of membrane locking and the increasing difference in the orders of the magnitudes between the transverse shear strain and its two parts can be a source of shear locking.

4.2. Detailed strain analysis using the MITC6 shell element

In the previous section, we identified why the free hyperboloid shell problem is difficult to solve accurately. We next perform the same analysis as in the previous section using a uniform 24×24 mesh of the MITC6 [12] triangular shell finite elements based on the basic shell mathematical model. Ref. [12] reports that for the free hyperboloid shell problem the 6-node element shows some locking when the shell thickness is very small.

As in Section 4.1, two cases of thickness, $t/L = 1/100$ and $t/L = 1/1000$, are considered. We show only the membrane and transverse shear strains and their parts because these were recognized as difficult to solve for. Indeed, the other strain components are accurately predicted in this solution.

Figs. 18 and 19 display the distributions of the strain components of the free hyperboloid shell problem when t/L is 1/100. In this case, the solutions of the membrane and transverse shear strains are reasonably smooth but (except for the strain component ϵ_{12}) less smooth than their parts. The magnitudes of the solutions except for the transverse shear strain ϵ_{13} (with predicted values however still reasonably small) are quite well predicted compared with the reference solutions.

Figs. 20 and 21 show the solutions when t/L is 1/1000. It is interesting to note that the distributions of the membrane and transverse shear strains are not smooth and the magnitudes of the solutions are not accurate although their parts (except for the strain component ϵ_{12}) are quite well approximated.

This numerical example using the MITC6 shell finite element demonstrates how the difficulty of calculating the strain components with large individual parts affects the finite element solution in the free hyperboloid shell problem. Clearly, the phenomenon we see is some membrane and shear locking.

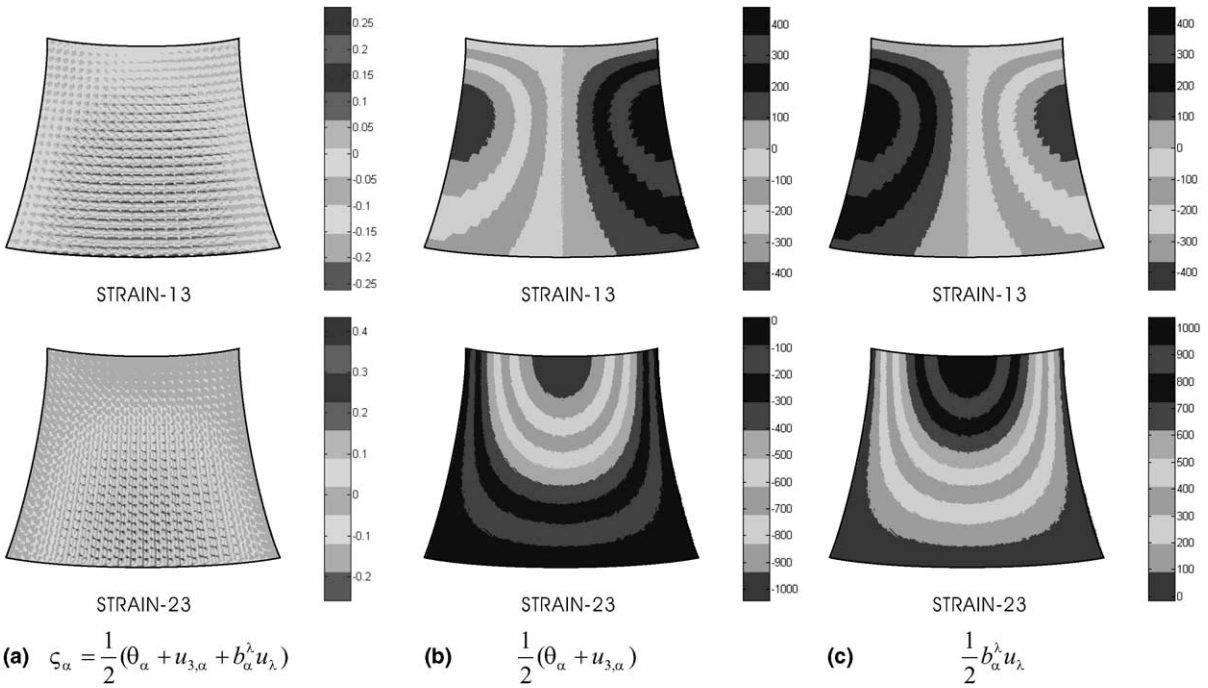

Fig. 21. Distributions of the strain components of the free hyperboloid shell problem calculated using the MITC6 shell element; $t/L = 1/1000$: (a) the transverse shear strain; (b) the first part of the transverse shear strain and (c) the second part of the transverse shear strain.

5. Conclusions

The objective of this paper was to obtain new insight into the finite element discretization and solution of shell structures. For this purpose, we used the basic shell mathematical model to formulate shell finite elements that are equivalent to the widely-used continuum mechanics based shell finite elements, including the MITC elements.

We showed that when finite elements are formulated based on a shell theory, it is important to ensure that the rigid body modes can be represented. If the interpolations used do not exactly admit rigid body modes, large errors can be present in the solution, in particular, if the shell is thin and a bending dominated condition is analyzed.

Considering shell analysis, it is well known that large differences in magnitudes of the strain terms and their parts can arise. We highlighted this fact in this paper and presented the analysis of a shell structure for which the membrane and shear strain components contain parts of large magnitudes. These individual parts are orders of magnitudes larger than the actual strain components and these orders of magnitude differences quickly increase as a shell thickness decreases. Since each of the parts is calculated from different displacement and rotation derivatives in the finite element solution, clearly difficulties in the development of effective shell elements must be anticipated and these relate to the well-known locking phenomena. While we concentrated here on the usually used five degrees-of-freedom per node continuum mechanics based shell elements, these observations are, of course, also applicable when considering 3D shell elements and their underlying mathematical model [27].

The insight provided in this study should help to improve the mixed interpolation of strain components, or develop interpolations for their individual parts, in order to arrive at improved shell analysis capabilities.

Appendix A. Axial strain of an *n*-node truss element

We discuss the difference arising in the axial strain of an n-node truss element when using the two displacement interpolations in Eqs. (39) and (51).

Let us consider the truss element oriented along the x_1-axis, see Fig. 22. We assume the interpolation of the geometry to be

$$\vec{x} = x_1\vec{i}_1 = \sum_{i=1}^{n} h_i(r)x_1^i\vec{i}_1, \tag{A.1}$$

where the $h_i(r)$ are the usual shape functions and x_1^i denotes the position of node i on the x_1-axis. The base vectors are given by

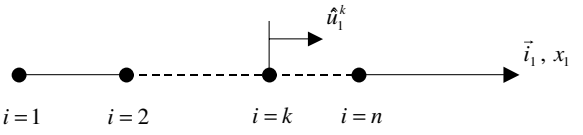

Fig. 22. An n-node truss element.

$$\vec{a}_1 = \frac{\mathrm{d}x_1}{\mathrm{d}r}\vec{i}_1 = \sum_{i=1}^{n}\frac{\mathrm{d}h_i}{\mathrm{d}r}x_1^i\vec{i}_1, \quad \vec{a}^1 = \frac{\mathrm{d}r}{\mathrm{d}x_1}\vec{i}_1. \tag{A.2}$$

For the displacement interpolation by Eqs. (38) and (39), the displacement field is given by

$$\vec{u} = \hat{u}_1\vec{i}_1 = \sum_{i=1}^{n} h_i(r)\hat{u}_1^i\vec{i}_1. \tag{A.3}$$

We obtain the axial (physical) strain corresponding to the x_1-direction as

$$\epsilon_{11} = \frac{\mathrm{d}\hat{u}_1}{\mathrm{d}x_1} = \frac{\mathrm{d}\hat{u}_1}{\mathrm{d}r}\frac{\mathrm{d}r}{\mathrm{d}x_1} = \frac{\mathrm{d}r}{\mathrm{d}x_1}\sum_{i=1}^{n}\frac{\mathrm{d}h_i}{\mathrm{d}r}\hat{u}_1^i. \tag{A.4}$$

Considering the displacement interpolation by Eqs. (37) and (51), the displacement field is given by

$$\vec{u} = u_1\vec{a}^1 = u_1\frac{\mathrm{d}r}{\mathrm{d}x_1}\vec{i}_1 = \frac{\mathrm{d}r}{\mathrm{d}x_1}\sum_{i=1}^{n} h_i u_1^i\vec{i}_1. \tag{A.5}$$

Using Eqs. (A.3) and (A.5), we have

$$\hat{u}_1 = \frac{\mathrm{d}r}{\mathrm{d}x_1}u_1 = \frac{\mathrm{d}r}{\mathrm{d}x_1}\sum_{i=1}^{n} h_i u_1^i. \tag{A.6}$$

The corresponding axial strain is obtained as

$$\begin{aligned}\epsilon_{11} &= \frac{\mathrm{d}\hat{u}_1}{\mathrm{d}r}\frac{\mathrm{d}r}{\mathrm{d}x_1}\\ &= \left\{\frac{\mathrm{d}}{\mathrm{d}r}\left(\frac{\mathrm{d}r}{\mathrm{d}x_1}\right)\sum_{i=1}^{n} h_i u_1^i + \frac{\mathrm{d}r}{\mathrm{d}x_1}\sum_{i=1}^{n}\frac{\mathrm{d}h_i}{\mathrm{d}r}u_1^i\right\}\frac{\mathrm{d}r}{\mathrm{d}x_1}.\end{aligned} \tag{A.7}$$

Since we have the relationship

$$u_1^i = \left(\frac{\mathrm{d}x_1}{\mathrm{d}r}\right)^i\hat{u}_1^i \tag{A.8}$$

at the nodes, the axial strain using Eqs. (37) and (51) is finally given in terms of $\hat{u}_1^i$ as

$$\begin{aligned}\epsilon_{11} = {}& \frac{\mathrm{d}}{\mathrm{d}r}\left(\frac{\mathrm{d}r}{\mathrm{d}x_1}\right)\left\{\sum_{i=1}^{n} h_i\left(\frac{\mathrm{d}x_1}{\mathrm{d}r}\right)^i\hat{u}_1^i\right\}\frac{\mathrm{d}r}{\mathrm{d}x_1}\\ &+ \left(\frac{\mathrm{d}r}{\mathrm{d}x_1}\right)^2\left\{\sum_{i=1}^{n}\frac{\mathrm{d}h_i}{\mathrm{d}r}\left(\frac{\mathrm{d}x_1}{\mathrm{d}r}\right)^i\hat{u}_1^i\right\}.\end{aligned} \tag{A.9}$$

Comparing Eqs. (A.4) and (A.9), it is clearly recognized that the two strain interpolations are not the same. We only obtain the same strains in case $\mathrm{d}x_1/\mathrm{d}r$ is constant in the element.

An important requirement for convergence of a finite element scheme is the possibility to represent the rigid

body modes. If we set all $\hat{u}_1^i$ equal to a constant value, the corresponding physical axial strain should be zero. This condition is obviously satisfied using the interpolation in Eq. (A.3) but not in general using Eq. (A.5).

We do not use an element which cannot represent the rigid body modes exactly. In case the rigid body modes cannot be represented, strain energy is stored in the element under rigid body motions. Such an element will in particular capture non-physical strain energy in bending dominated problems (see Fig. 6(b)) and in large displacement analysis.

References

[1] Bathe KJ. Finite element procedures. New York: Prentice Hall; 1996.

[2] Chapelle D, Bathe KJ. The finite element analysis of shells—fundamentals. Berlin: Springer-Verlag; 2003.

[3] Chapelle D, Bathe KJ. The mathematical shell model underlying general shell elements. Int J Numer Methods Eng 2000;48:289–313.

[4] Chapelle D, Bathe KJ. Fundamental considerations for the finite element analysis of shell structures. Comput Struct 1998;66:19–36. 711–2.

[5] Lee PS, Bathe KJ. On the asymptotic behavior of shell structures and the evaluation in finite element solutions. Comput Struct 2002;80:235–55.

[6] Bathe KJ, Chapelle D, Lee PS. A shell problem 'highly sensitive' to thickness changes. Int J Numer Methods Eng 2003;57:1039–52.

[7] Pitkäranta J, Sanchez-Palencia E. On the asymptotic behaviour of sensitive shells with small thickness. CR Acad Sci II 1997;325:127–34.

[8] Baiocchi C, Lovadina C. A shell classification by interpolation. Math Mod Methods Appl Sci 2002;12:1359–80.

[9] Dvorkin EN, Bathe KJ. A continuum mechanics based four-node shell element for general nonlinear analysis. Eng Comput 1984;1:77–88.

[10] Bathe KJ, Dvorkin EN. A formulation of general shell elements—the use of mixed interpolation of tensorial components. Int J Numer Methods Eng 1986;22:697–722.

[11] Bucalem ML, Bathe KJ. Higher-order MITC general shell elements. Int J Numer Methods Eng 1993;36:3729–54.

[12] Lee PS, Bathe KJ. Development of MITC isotropic triangular shell finite elements. Comput Struct 2004;82:945–62.

[13] Bathe KJ, Iosilevich A, Chapelle D. An inf–sup test for shell finite elements. Comput Struct 2000;75:439–56.

[14] Bathe KJ, Iosilevich A, Chapelle D. An evaluation of the MITC shell elements. Comput Struct 2000;75:1–30.

[15] Bathe KJ. The inf–sup condition and its evaluation for mixed finite element methods. Comput Struct 2001;79:243–52. 971.

[16] Hiller JF, Bathe KJ. Measuring convergence of mixed finite element discretizations: an application to shell structures. Comput Struct 2003;81:639–54.

[17] Noor AK, Belytschko T, Simo JC. editors. Analytical and computational models of shells. ASME CED-Vol 3; 1989.

[18] Büchter N, Ramm E. Shell theory versus degeneration—a comparison in large rotation finite element analysis. Int J Numer Methods Eng 1992;34:39–59.

[19] Bernadou M. Finite element methods for thin shell problems. Chichester: Wiley; 1996.

[20] Destuynder P, Salaün M. A mixed finite element for shell model with free edge boundary conditions. Part 3. Numerical aspects. Comput Methods Appl Mech Eng 1996;136:273–92.

[21] Ibrahimbegović A. Stress resultant geometrically exact shell theory for finite rotations and its finite element implementation. Appl Mech Rev 1997;50:199–226.

[22] Başar Y, Krätzig WB. Theory of shell structures. 2nd ed. Düsseldorf: Fortschritts-Berichte VDI; 2001.

[23] Krätzig WB, Jun D. On 'best' shell models—from classical shells, degenerated and multi-layered concepts to 3D. Arch Appl Mech 2003;73:1–25.

[24] Cho M, Roh HY. Development of geometrically exact new shell elements based on general curvilinear co-ordinates. Int J Numer Methods Eng 2003;56:81–115.

[25] Chapelle D, Oliveira DL, Bucalem ML. MITC elements for a classical shell model. Comput Struct 2003;81:523–33.

[26] Bathe KJ, Lee PS, Hiller JF. Towards improving the MITC9 shell element. Comput Struct 2003;81:477–89.

[27] Chapelle D, Ferent A, Bathe KJ. 3D-shell elements and their underlying mathematical model. Math Models Methods Appl Sci 2004;14:105–42.